

# Towards Robust Red-Green Watermarking for Autoregressive Image Generators

Denis Lukovnikov\*

Andreas Müller\*

Erwin Quiring

Asja Fischer

Ruhr-University Bochum, Germany

denis.lukovnikov, andreas.mueller-tlx, erwin.quiring, asja.fischer}@rub.de

## Abstract

*In-generation watermarking for detecting and attributing generated content has recently been explored for latent diffusion models (LDMs), demonstrating high robustness. However, the use of in-generation watermarks in autoregressive (AR) image models has not been explored yet. AR models generate images by autoregressively predicting a sequence of visual tokens that are then decoded into pixels using a vector-quantized decoder. Inspired by red-green watermarks for large language models, we examine token-level watermarking schemes that bias the next-token prediction based on prior tokens. We find that a direct transfer of these schemes works in principle, but the detectability of the watermarks decreases considerably under common image perturbations. As a remedy, we propose two novel watermarking methods that rely on visual token clustering to assign similar tokens to the same set. Firstly, we investigate a training-free approach that relies on a cluster lookup table, and secondly, we finetune VAE encoders to predict token clusters directly from perturbed images. Overall, our experiments show that cluster-level watermarks improve robustness against perturbations and regeneration attacks while preserving image quality. Cluster classification further boosts watermark detectability, outperforming a set of baselines. Moreover, our methods offer fast verification runtime, comparable to lightweight post-hoc watermarking.*

## 1. Introduction

The watermarking of AI-generated content is a key tool to address misuse [19], to achieve content authenticity, and to maintain the quality of training data by filtering out AI-generated material. Besides classic post-hoc watermarking, one line of research explores techniques for embedding watermarks already during the generation process. Most research has focused on diffusion models [10, 31, 36], while autoregressive (AR) image models have received less attention so far. However, recent progress in AR models and their assumed usage by the recent GPT 4o model [35]



Figure 1. Watermarking for autoregressive models by biasing token selection. The watermark is deeply embedded in the image’s token composition, changing its appearance.

strongly motivate a more comprehensive exploration of watermarks for AR image models.

AR models for image generation [2, 3, 9, 17, 24, 26, 27, 29, 30, 38, 39] generate images by predicting a sequence of tokens in a latent space that is then transformed to pixels using a decoder. A common approach is to use discrete tokens which are obtained after a quantization of the latent space. In the following, we focus on such AR image models that use discrete tokens in the latent space.

In this work, we explore the embedding of watermarks during the autoregressive generation process. To this end, we consider token-level watermarks which have been previously investigated in the context of text generation with large language models (LLMs). In particular, we adopt the red-green watermarking approach proposed by Kirchenbauer et al. [14] due to its simplicity and effectiveness. This approach builds on the idea of partitioning tokens into red and green sets, then biasing the model to favor green tokens during generation. This enables watermark detection by counting the proportion of green tokens in a given text.

As a baseline, we first examine the direct transfer of red-green watermarks. Although this approach works in principle, we find that the watermarks lack robustness under common image perturbations. This can be explained by the following observations: To verify the watermark, a given image needs to be mapped back to the tokens that were originally decoded by the AR model to produce the image. Firstly, the tokens might not be perfectly recon-

\*Equal contribution

structed due to a mismatch between the VQVAE’s image encoding and decoding models. Secondly, image perturbations further amplify the discrepancy between the original and the reconstructed tokens. Hence, a naive application of red-green LLM watermarks is not a suitable approach for image generators.

As a remedy, we introduce a new watermarking concept based on visual token clustering. By clustering similar tokens together and building the green and red set on cluster level instead of token level, the watermark detection robustness improves considerably. Even after image perturbations (e.g. blur), the reconstructed tokens are more likely to fall into the same cluster as the originally generated tokens.

We realize our clustering concept in two variants. First, we propose a training-free watermarking approach where determine whether a token is green based on its cluster. Second, to further boost watermark robustness, we also investigate finetuning VAE encoders to directly predict clusters given an image instead of tokens (*Cluster Classifier*).

In summary, our contributions are as follows:

- **Red-Green Watermarking for AR Image Models.** We are among the first to investigate red-green watermarking for AR image models and propose two novel approaches based on token clustering.
- **Robustness Analysis.** We conduct an extensive robustness analysis demonstrating the high robustness of our novel approaches against common image perturbations.
- **Extensive Evaluation.** We thoroughly evaluate the proposed techniques on different left-to-right autoregressive image models, i.e., LlamaGen [24] (versions GPT-B and GPT-L) and RAR-XL [39].

## 2. Preliminaries

We start by revisiting AR image generation and red-green text watermarking for LLMs.

### 2.1. Autoregressive Image Generation

There are various works [2, 3, 9, 17, 24, 26, 27, 29, 30, 38, 39] that have developed autoregressive methods for image generation with different sampling approaches. In the following, we focus on the common approach of decoding discrete tokens from a latent space, that is, on approaches that rely on vector-quantized variational autoencoders (VQ-VAE) for mapping images to a sequence of tokens and vice versa.

Here, a color image  $x \in \mathbb{R}^{3 \times H \times W}$  is first mapped to a latent space using an encoder  $\mathcal{E}$ , resulting in continuous feature vectors  $\mathcal{E}(x) = z \in \mathbb{R}^{d \times h \times w}$ . This latent representation is then quantized to visual tokens  $q \in \mathbb{V}^{h \times w}$  based on

a codebook. More precisely, there exists a fixed vocabulary  $\mathbb{V}$  with a corresponding codebook  $\mathbb{Q} \in \mathbb{R}^{|\mathbb{V}| \times d}$  containing  $d$ -dimensional vectors. These vectors are used to look up the nearest token to each of the  $h \times w$   $d$ -dimensional vectors in  $z$ , obtaining the collection of visual tokens  $q$ . The tokens can be mapped back to an image by first dequantizing them using the same codebook  $\mathbb{Q}$  and then mapping the latent vectors into pixel space using a corresponding decoder  $D : \mathbb{R}^{d \times h \times w} \rightarrow \mathbb{R}^{3 \times H \times W}$ .

An autoregressive image generator models the joint distribution of image tokens  $p(q_1, q_2, \dots, q_{h \cdot w} | c)$  given a context  $c$  (such as a class or text) by decomposing it into  $\prod_i^{h \cdot w} p_\theta(q_i | q_{<i}, c)$ . Here,  $\theta$  denotes the the model parameters that are fitted during training. During generation, a sequence of tokens is subsequently generated by sampling from  $p_\theta$  at every step. The default setting is to generate an image by producing tokens describing parts of the image, in a left-to-right, top-down scanning order. We therefore consider this setting for our watermarking approach. Note, however, that alternative orderings and parallel decoding [2, 3, 17, 27] have also been explored.

### 2.2. Red-Green Watermarking

Several methods have been proposed to watermarking LLM-generated text [4, 14, 15, 16, 21, 32, 37]. In this work, we adopt the red-green watermarking technique from Kirchenbauer et al. [14] due to its simplicity and effectiveness. At every generation step, this technique uses the previously decoded tokens to seed a random function that is used to partition the vocabulary of the generator into two sets, one referred to as “green”, the other referred to as “red”. More formally, given the sequence of tokens decoded so far,  $y_{<i} = (y_1, \dots, y_{i-1}) \in \mathbb{V}^{n-1}$ , we first compute a hash  $o_i = \text{hash}(y_{i-1}, \dots, y_{i-l}, \kappa)$  using a random hashing function like SHA256. Here,  $\kappa$  is a predefined secret key that remains the same across multiple generations, and  $l$  is the number of preceding tokens that are used. The hash  $o_i$  is then used to seed a pseudorandom number generator (PRNG) that is then used to randomly select a fraction  $\gamma$  of tokens from  $\mathbb{V}$  to form the set of green tokens  $G_i$  of size  $\lfloor \gamma * |\mathbb{V}| \rfloor$ . The red set of tokens is then its complement:  $R_i = \mathbb{V} \setminus G_i$ . Given  $G_i$ , the bias mask  $m_i \in \{0, 1\}^{\mathbb{V}}$  is defined by setting the mask to one for green tokens:  $m_i[v] = \mathbf{1}_{G_i}(v)$ . Next, the model’s distribution over  $\mathbb{V}$  is biased to favor tokens from the green set by adding some value  $\delta$  to their logits  $f_\theta(y_{<i}) \in \mathbb{R}^{\mathbb{V}}$  predicted by the model before normalizing them using the softmax function, that is

$$p'_\theta(y_i | y_{<i}) = \text{softmax}(f_\theta(y_{<i}) + m_i * \delta) .$$

The smaller the value of  $\delta$  is, the less the generator’s distribution is affected, but the weaker the watermark signal.

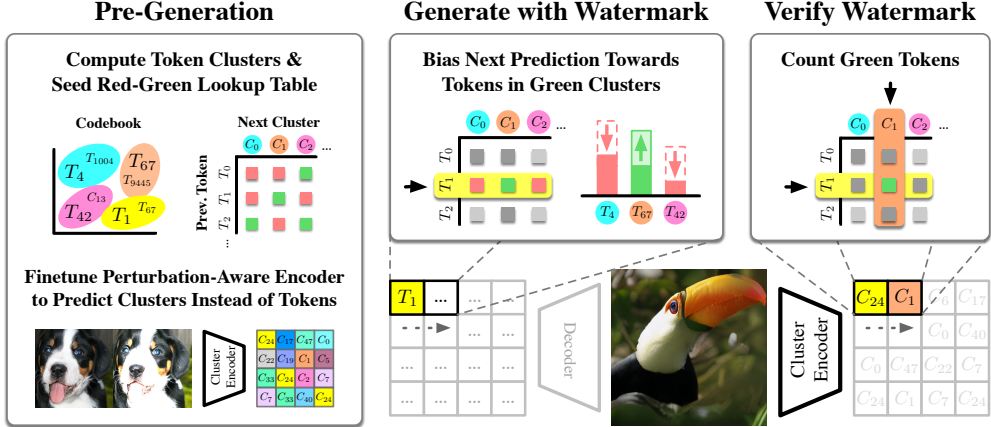


Figure 2. Overview of our proposed cluster-based red-green watermarking for AR models.

In order to verify the watermark for the given sequence  $(y_1, \dots, y_T)$ , we can simply recompute the green sets  $G_i$  for every given token given the preceding context. This is fast as there is no need to access the original model. Finally, we perform an one-tailed statistical test that is based on determining how unlikely it is to observe the given number of green tokens,  $\#_{\text{green}}$ , in the entire sequence by chance. The null hypothesis here is that the observed number of green tokens is distributed according to an unbiased binomial distribution:  $H_0 : \#_{\text{green}} \sim \text{Binomial}(T, \gamma)$ .  $H_0$  is rejected for a sequence if its p-value exceeds a chosen threshold  $\rho$ .

### 3. Red-Green Watermarks for AR Image Generators

We begin by outlining the naive approach of directly applying red-green watermarking to autoregressive image models. Next, we introduce our clustering-based token grouping to enhance robustness, followed by our fine-tuning strategy.

#### 3.1. Basic Red-Green AR Watermarking

As a **baseline** variant, we consider the naive application of LLM red-green watermarking on the token sequence  $\{q_i\}_1^{h,w} = (q_1, \dots, q_{h,w})$  produced by the AR image generation model. The **generation** of the image consists of two phases: (1) sampling the token sequence  $\{q_i\}_1^{h,w}$  using the AR model, and (2) mapping the token sequence to an image  $x$  using the VQ-VAE. During sampling, the hash for the red-green partitioning is computed from the previous token:  $o_i = \text{hash}(\kappa, q_{i-1})$ . We refer to  $\kappa$  as the (hash) prefix. For the **verification** of a given image  $x$ , we first use the encoder and quantizer of the VQ-VAE to produce a token sequence  $\{q'_i\}_1^{h,w}$ , and then count the fraction of green tokens along the generation order.

### 3.2. Cluster-Based Red-Green AR Watermarking

Due to the quantization in the encoding step of the VQ-VAE, even small image perturbations can lead to entirely different tokens being predicted for a large fraction of the tokens (since it is sufficient that the perturbation moves the latent presentation closer to another token in the codebook). This sensitivity of the token reconstruction leads to poor robustness under image perturbations, because similar tokens are randomly assigned to either red or green sets. Thus, we examine clustering tokens in the codebook by their embeddings to improve robustness. Tokens are partitioned into green and red sets such that all tokens belonging to the same cluster are either in the green or in the red set.

**Clustering the Vocabulary.** Before generation, we first use  $k$ -means to partition the vocabulary  $\mathbb{V}$  into  $k$  non-overlapping sets of tokens based on the Euclidean distance between vectors provided by the codebook  $\mathbb{Q}$ , resulting in a set of clusters  $(C_1, \dots, C_k)$ . In the following, using a slightly overloaded notation, we denote the cluster lookup function as  $C[q]$ , which returns the id of the cluster to which the token  $q$  has been assigned.

**Watermarking with Clusters.** During **generation**, there are two main differences compared to the basic case. The hash  $o_i$  is computed based on the cluster of the preceding token:  $o_i = \text{hash}(\kappa, C[q_{i-1}])$ , where  $\kappa$  is the (hash) prefix that is kept constant across multiple generations. The hash is then used to compute a green set  $G_i^{\text{cluster}}$  over clusters  $(C_1, \dots, C_k)$ , rather than over the vocabulary  $\mathbb{V}$ . The green set over  $\mathbb{V}$  is simply the union over green clusters:  $G_i = \bigcup_{C_i \in G^{\text{cluster}}} C_i$ . This green set of tokens  $G_i$  is then used like the token-level green sets in the basic case to bias the generative distribution towards generating one of the green tokens. Note that all tokens in a cluster get the same

red/green set assignment, which should improve robustness, assuming that similar tokens are decoded after image perturbation. **Verification** works similar to the verification procedure in the basic variant with the difference that hashing and masking are again done on cluster level.

Algorithm 1 describes the generation and verification process in detail.

### 3.3. Cluster Classifier

The approach discussed so far is training-free and only relies on the clustering of tokens based on their codebook vectors. As an extension of this cluster-based watermarking approach, we also investigate **finetuning** the VAE encoder to obtain a **Cluster Classifier (CC)**. Given an image, it directly predicts the clusters of the tokens at every position, rather than trying to reconstruct the original tokens. Finetuning is done adversarially with perturbation-augmented images to further boost robustness.

The Cluster Classifier  $\mathcal{M}$  is implemented by taking a copy of the VQ-VAE encoder  $\mathcal{E}$  without the pre-quantization layer, and adding a simple classification output layer for  $k$  classes. The CC is finetuned using unwatermarked images generated by the AR model. The Cluster Classifier is then supervised to predict the clusters of the original tokens, which translates to the following objective:

$$\mathcal{L}_{\text{CC}} = \mathbb{E}_{(x, \{q_i\})^{h \cdot w} \sim p_\theta} \left[ \sum_i \text{CE}(\mathcal{M}(\phi(x))_i, C[q_i]) \right], \quad (1)$$

where  $\text{CE}(\cdot)$  is the cross-entropy loss and  $\phi(\cdot)$  is a perturbation function that applies one perturbation from a predefined set of perturbations on a given image. Note that the cross-entropy is computed for every token individually and is then averaged over all tokens in an image. The clusters  $C_i$  are created using k-means as in the training-free approach. Moreover, the use of the Cluster Classifier does not require any changes to the watermarking procedure when generating images and can be simply applied for verification.

### 3.4. Prefix Tuning

In our early experiments, we noticed that the prefix  $\kappa$  used with the hashing function can have a significant effect on watermark detection performance. This effect is especially pronounced for extremely low numbers of clusters but still has some effect when 64 or 128 clusters are used. Therefore, we propose to perform a simple search to empirically identify the best performing prefixes. This can be done by generating a small set of images with different prefixes, and evaluating the robustness of the watermark under various perturbations, retaining and deploying the best prefixes.

---

### Algorithm 1 Cluster-Based Red-Green Watermarking

---

```

1: function COMPUTEGREENSET( $q_{<i}, \mathbb{V}, C, \kappa, \gamma$ )
2:   context  $\leftarrow C[q_{-1}]$                                  $\triangleright$  Get last cluster
3:    $\mathcal{G} \leftarrow \text{PRNG}(\text{hash}(\kappa, \text{context}))$        $\triangleright$  Seed PRNG
4:   for  $j = 1, 2, \dots, k$  do
5:      $r_j \leftarrow \mathcal{G}.\text{uniform}(0, 1)$ 
6:   end for
7:    $k_{\text{green}} \leftarrow \lfloor \gamma \cdot k \rfloor$                  $\triangleright$  Number of green clusters
8:    $G^{\text{cluster}} \leftarrow \text{argsort}((r_1, r_2, \dots, r_k))[:k_{\text{green}}]$ 
9:    $G = \bigcup\{C_j : C_j \in G^{\text{cluster}}\}$              $\triangleright$  Merge green
10:  return  $G$ 
11: end function

12: function GENERATEWITHWM( $p_\theta, \mathbb{V}, C, \kappa, \gamma, \delta, c$ )
13:    $q_1 \sim p_\theta(c)$                                  $\triangleright$  Sample first token
14:   for  $i = 2, \dots, h.w$  do       $\triangleright$  Generate  $h.w$  tokens
15:      $G_i \leftarrow \text{ComputeGreenSet}(q_{<i}, \mathbb{V}, C, \kappa, \gamma)$ 
16:      $l_i \leftarrow f_\theta(q_{<i}, c)$                        $\triangleright$  Compute model logits
17:     for  $v \in G_i$  do
18:        $l_i[v] \leftarrow l_i[v] + \delta$                    $\triangleright$  Bias green
19:     end for
20:      $q_i \sim \text{softmax}(l_i)$                        $\triangleright$  Sample next token
21:   end for
22:   return  $x_{1:n}$ 
23: end function

24: function VERIFYWATERMARK( $q_{1:h.w}, \mathcal{V}, C, \kappa, \gamma$ )
25:   green_count  $\leftarrow 0$ 
26:   for  $i = 2, \dots, h.w$  do     $\triangleright$  Start from second token
27:      $G_i \leftarrow \text{ComputeGreenSet}(q_{<i}, \mathbb{V}, C, \kappa, \gamma)$ 
28:     if  $q_i \in G_i$  then
29:       green_count  $\leftarrow$  green_count + 1
30:     end if
31:   end for
32:    $p\text{-value} \leftarrow 1 - \text{CDF}_{\text{Binom}}(\text{green\_count} - 1, h.w, \gamma)$ 
33:   return  $p\text{-value}$ 
34: end function

```

---

## 4. Experiments

We proceed with an empirical evaluation of the proposed red-green AR watermarking techniques.

### 4.1. Experimental Setup

**Models.** We conduct experiments on two left-to-right autoregressive model: LlamaGen [24] and RAR [39]. For both models, their class-to-image variants are used, which generate images for ImageNet [23] classes. The best reported settings in their papers or code are used when generating images. See Table 3 in Supplementary Material for details.

Model	FID $\downarrow$	Clean	JPEG 20	Gauss. Blur R 3	Gauss. std .2	Salt&Pepper .1	Color Jitter	Regeneration
LlamaGen GPT-B 256 $\times$ 256 (Baseline FID=6.01)								
DWT-DCT	6.02	0.960 — 0.837	0.496 — 0.008	0.500 — 0.013	0.485 — 0.009	0.511 — 0.011	0.568 — 0.209	0.519 — 0.016
DWT-DCT-SVD	6.51	1.000 — 1.000	0.415 — 0.006	0.975 — 0.785	0.503 — 0.005	0.506 — 0.009	0.542 — 0.161	0.826 — 0.494
RivaGAN	6.34	1.000 — 0.999	0.928 — 0.510	0.996 — 0.963	0.951 — 0.661	0.958 — 0.701	0.848 — 0.752	0.853 — 0.475
IndexMark (+IE)	5.84	1.000 — 1.000	0.969 — 0.821	0.761 — 0.171	0.631 — 0.055	0.635 — 0.071	0.907 — 0.732	0.951 — 0.761
Ours (No Clustering)	5.90	0.999 — 0.996	0.922 — 0.680	0.623 — 0.068	0.624 — 0.070	0.623 — 0.080	0.851 — 0.573	0.916 — 0.710
Ours (Clustering, k=64)	6.12	1.000 — 1.000	0.993 — 0.959	0.950 — 0.691	0.860 — 0.414	0.876 — 0.427	0.930 — 0.806	0.997 — 0.972
+ CC (k=64)	6.12	1.000 — 1.000	0.985 — 0.906	0.991 — 0.928	0.986 — 0.900	1.000 — 0.999	0.985 — 0.957	0.993 — 0.935
LlamaGen GPT-L 384 $\times$ 384 (Baseline FID=4.50)								
DWT-DCT	4.36	0.932 — 0.800	0.502 — 0.011	0.526 — 0.018	0.490 — 0.011	0.499 — 0.013	0.566 — 0.224	0.538 — 0.027
DWT-DCT-SVD	4.54	1.000 — 0.999	0.461 — 0.010	0.975 — 0.815	0.518 — 0.009	0.502 — 0.008	0.544 — 0.195	0.888 — 0.628
RivaGAN	4.62	1.000 — 0.999	0.958 — 0.702	0.999 — 0.983	0.950 — 0.682	0.959 — 0.733	0.859 — 0.790	0.910 — 0.596
IndexMark (+IE)	4.49	0.999 — 0.999	0.976 — 0.836	0.841 — 0.307	0.642 — 0.035	0.654 — 0.041	0.929 — 0.793	0.983 — 0.834
Ours (No Clustering)	4.36	1.000 — 1.000	0.961 — 0.836	0.716 — 0.203	0.653 — 0.097	0.643 — 0.090	0.884 — 0.683	0.961 — 0.812
Ours (Clustering, k=64)	4.85	1.000 — 1.000	0.995 — 0.979	0.976 — 0.890	0.886 — 0.460	0.918 — 0.518	0.925 — 0.838	0.999 — 0.997
+ CC (k=64)	4.85	1.000 — 1.000	0.989 — 0.936	0.996 — 0.982	0.991 — 0.947	1.000 — 1.000	0.983 — 0.963	0.999 — 0.989
RAR-XL 256 $\times$ 256 (Baseline FID=3.13)								
DWT-DCT	3.29	0.976 — 0.883	0.500 — 0.008	0.511 — 0.014	0.488 — 0.006	0.520 — 0.009	0.574 — 0.224	0.534 — 0.013
DWT-DCT-SVD	3.87	1.000 — 1.000	0.411 — 0.003	0.983 — 0.802	0.504 — 0.004	0.494 — 0.004	0.534 — 0.135	0.819 — 0.462
RivaGAN	3.64	1.000 — 1.000	0.943 — 0.550	0.998 — 0.983	0.956 — 0.651	0.963 — 0.730	0.860 — 0.785	0.870 — 0.496
Ours (No Clustering)	3.14	1.000 — 1.000	0.930 — 0.624	0.641 — 0.074	0.502 — 0.023	0.533 — 0.031	0.865 — 0.548	0.949 — 0.764
Ours (Clustering, k=64)	3.96	1.000 — 1.000	0.992 — 0.922	0.778 — 0.163	0.717 — 0.138	0.754 — 0.140	0.936 — 0.696	0.987 — 0.893
+ CC (k=64)	3.96	1.000 — 1.000	0.994 — 0.958	0.982 — 0.811	0.972 — 0.820	1.000 — 0.998	0.985 — 0.940	0.991 — 0.923

Table 1. Main results on a challenging set of perturbations. See Table 5 in Supplementary Material for detailed perturbation settings. We report AUC — TPR@FPR=1% across various perturbations and regeneration attacks. For our method *Ours (No Clustering)*, we set a penalty  $\delta = 5$  and the green token fraction  $\gamma = 0.25$ . For *Ours (Clustering)* and for our method using the cluster classifier (+ CC), we use  $k = 64$  clusters, and  $\delta = 5, \gamma = 0.25$ .

**Settings and Metrics.** We evaluate our watermarking techniques empirically by generating 2.000 watermarked images and computing ROC statistics on the fraction of green tokens against a set of 2.000 generated images without watermarks. Results are reported as AUC and TPR@FPR=1. We explore different settings for the cluster-based watermark by varying the number of clusters ( $k \in \{8, 16, 32, 64, 128\}$ ). We also try different strengths for the watermark ( $\delta \in \{2, 5\}$ ) as well as different fractions of green tokens ( $\gamma \in \{0.5, 0.25\}$ ). This is done for different hash prefixes ( $\kappa \in \{1, \dots, 8\}$ ) from which we pick the best performing prefixes (see Table 7 in the Supplementary Material). To evaluate image quality, we calculate the FID [12] using 50k generated images against the ImageNet validation set.

**Robustness Analysis.** The robustness is evaluated w.r.t. both perturbations and regeneration attacks. We use an extensive set of image perturbations, such as Gaussian Noise and Blur (see Table 4 in Supplementary Material for detailed settings). For regeneration attacks, we use the SD1.5 and FLUX.1 autoencoders, re-generating the watermarked images by first feeding them into the VAE’s encoder, and then decoding the obtained latent using the VAE decoder. We also test against the diffusion-based regeneration attack [41] with default settings, i.e. 60

steps of denoising using Stable Diffusion 2.1 [22]. Visual examples of all applied perturbations can be found in Figure 6 in Supp. Material.

**Baselines.** At the time of writing, there are no published watermarking methods for AR models. Hence, we compare our proposed AR watermark techniques with classic post-hoc watermarks: DWT-DCT [1], DWT-DCT-SVD [20], and RivaGAN [40]. These watermarks are applied to 2.000 unwatermarked images generated by each model. For LlamaGen, we also include the concurrent work of Tong et al. [28] (IndexMark) in the comparison, evaluating their published code with Index Encoder enabled (+IE). Since the authors don’t provide code or results for RAR, we do not evaluate IndexMark on RAR-XL.

**Training details.** To fine-tune the cluster classifier, we use 100k images generated using the model *without* applying watermarks. A predefined set of 64 clusters is used, obtained by k-means clustering. The model was finetuned for 30 epochs with batch size 16, which took  $\sim$ 12 hours on one A40 GPU. The set of perturbations used during finetuning is given in Table 6 in Supplementary Material. We use a perturbation schedule that increases the intensity of perturbations linearly during finetuning.

## 4.2. Results

Table 1 shows our main results. The reported watermarking hyper-parameters ( $k = 64$ ,  $\delta = 5$ ,  $\lambda = 0.25$ ) are determined by choosing the best trade-off between image quality (measured using FID) and robustness. See ablations below for further details on the selection. Overall, the results indicate that the cluster-based watermarking indeed significantly improves robustness, even in its training free variant. When combined with a cluster classifier (+ CC), it achieves the best overall results in the comparison. Visual examples of generated images are provided in Figures 9 to 11 in the Supplementary Material.

**Baseline Variant.** The simple token-level red-green watermark method (*Ours (No clustering)*) shows nearly perfect TPR@FPR1% in the clean setting, with image quality matching that of non-watermarked images, as measured by FID. However, under even mild image perturbations, such as Gaussian noise, TPR significantly drops, rendering the watermark unusable.

**Effect of Clustering.** The training-free cluster-based approach (*Ours (Clustering)*) drastically increases robustness against various perturbations for both LlamaGen variants as well as RAR-XL. While watermark detectability is significantly improved, robustness to blurring and salt-and-pepper noise remain hard to achieve. However, note that blurring and salt-and-pepper noise are very noticeable and destructive (see Figure 6 in the Supplementary Material for an example), which severely limits the usefulness of the perturbed image. With a sufficiently large number of clusters ( $k=64$  in Table 1), the FID remains low.

**Effect of Cluster Classifier.** Using the *cluster classifier* (+ CC) boosts robustness to several image perturbations for all studied models, beating all baselines. The effect is most pronounced for salt-and-pepper noise, color jitter, and blurring, which are also the most destructive transformations for our training-free variants. For example, the CC successfully learned to undo salt-and-pepper noise, yielding near-perfect watermark detection, up from 14-52% TPR@1%FPR when only using clusters ( $k=64$ ).

**Comparison to baselines.** Results indicate that our best method beats all baselines, including the concurrent Index-Mark, by a large margin across all models on all perturbations except for Blur, which is especially vulnerable at lower resolutions.

**Verification Runtime.** Table 2 shows the runtime of the methods evaluated in this work. Time is measured by running watermark verification on single-example batches

for 1.000 images. For the baselines, we use a commonly used implementation for post-hoc watermarks and enable GPU-acceleration for RivaGAN.<sup>1</sup> The results indicate that token-based watermarks for AR models, such as ours, can be as fast as simple DWT-DCT watermarking (10-25 milliseconds). This is in stark contrast to recently proposed in-generation watermarking methods for diffusion models (e.g., Tree-Ring [31]), which in addition to encoding the image to latent space also require full inversion of the diffusion process, incurring roughly the same time and energy overhead for verification as for generation. Note that we expect other red-green watermarking schemes to show similarly fast verification when efficiently implemented.

## 4.3. Ablation Study

We investigate the effect of the number of clusters  $k$ , watermarking strength (or penalty)  $\delta$ , and green token fraction  $\gamma$  on the TPR@FPR=1% under various perturbations in Figure 3 and on FID in Figure 4. While here we report only results for LlamaGen (GPT-L) and RAR-XL, and for TPR’s only the  $\gamma = 0.25$  setting, the full results can be found in the Supplementary Material (Figures 7 and 8).

**Effect of the number of clusters.** We tested extremely low numbers of clusters (down to 8) in order to study its effects on image degradation and watermark robustness. From the TPR plots in Figure 3, we can see that generally, a lower number of clusters results in higher robustness to various perturbations. This matches our expectations since larger clusters mean that the reconstructed tokens are less likely to leave their original token’s cluster after stronger perturbations. However, we also see a higher variance across different prefixes. The FID results reported in Figure 4 indicate that with a number of clusters lower than 64, there can be a significant increase in FID, resulting from reduced generation quality.

**Effect of green token fraction  $\gamma$  and penalty  $\delta$ .** Regarding image quality, we observe that  $\gamma = 0.25$  results in worse FID scores compared to  $\gamma = 0.5$ , especially when combined with a stronger penalty at extremely low numbers of clusters. Under the settings in Table 1 ( $k = 64$ ), it appears that  $\delta$  and  $\gamma$  don’t have a large effect on generation quality.

Regarding robustness, it is clear that a higher penalty value  $\delta$  always results in higher watermark robustness. The effect of the green set fraction  $\gamma$  can be seen in Figure 8 in supplementary material, which shows that  $\gamma = 0.25$  results in significantly higher robustness.

<sup>1</sup><https://github.com/ShieldMnt/invisible-watermark>

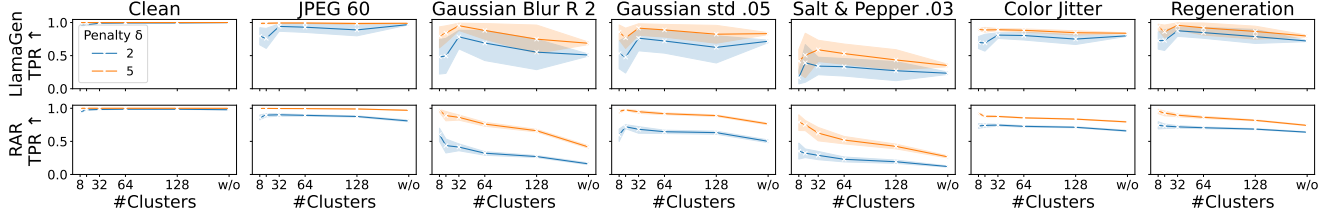


Figure 3. Empirical TPR@FPR=1% under different perturbations for LlamaGen (GPT-L) and RAR-XL for different numbers of clusters  $k$  and penalties  $\delta$ , with green token fraction  $\gamma$  set to 0.25 for the training-free approach. Results are reported over multiple prefixes (8 for RAR-XL and LlamaGen), lines indicate the average and shaded areas the standard deviation. See Figure 8 in the supplementary material for full results for all settings.

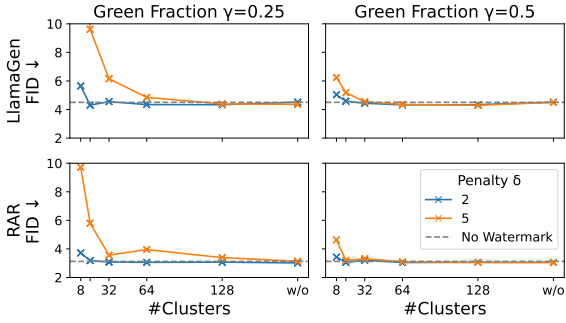


Figure 4. FID scores obtained for LlamaGen (GPT-L) and RAR-XL across different number of clusters  $k$ , different fractions of green tokens  $\gamma$  and penalties  $\delta$ . See Figure 7 in the supplementary material for full results for all settings.

Model	LlamaGen		RAR-XL
	(GPT-B) 256 × 256	(GPT-L) 384 × 384	256 × 256
Ours	$0.0123 \pm 1.09 \times 10^{-2}$	$0.0236 \pm 1.08 \times 10^{-2}$	$0.0149 \pm 1.32 \times 10^{-2}$
Ours (+ CC)	$0.0128 \pm 1.03 \times 10^{-2}$	$0.0227 \pm 8.41 \times 10^{-3}$	$0.0096 \pm 8.55 \times 10^{-3}$
DWT-DCT	$0.0093 \pm 3.36 \times 10^{-3}$	$0.0232 \pm 5.86 \times 10^{-3}$	$0.0115 \pm 5.48 \times 10^{-3}$
DWT-DCT-SVD	$0.0265 \pm 1.17 \times 10^{-2}$	$0.0684 \pm 2.69 \times 10^{-2}$	$0.0237 \pm 9.86 \times 10^{-3}$
RivaGAN	$0.0248 \pm 1.36 \times 10^{-2}$	$0.0615 \pm 2.04 \times 10^{-2}$	$0.0576 \pm 2.37 \times 10^{-2}$

Table 2. Comparison of verification runtime of our methods against baselines across different models and image sizes.

**Effect of hash prefix.** The effect of the prefix used when seeding the pseudo-random number generator for computing the green sets can have a significant effect on robustness. As shown in Figure 3, this effect is especially pronounced for lower numbers of clusters. The robustness to some perturbations, like salt-and-pepper noise and blur, is especially prone to this effect.

To investigate this, we examined the distributions of the number of green tokens when attempting to verify watermarks in watermarked and unwatermarked images. Ideally, the distribution of green token counts should center around 0.5 (for  $\gamma = 0.5$ ) for unwatermarked images. However, we observed that for low numbers of clusters, this assumption is not valid. An example is shown in Figure 5, comparing two

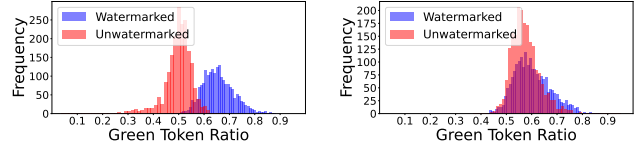


Figure 5. Distribution of green token ratio measured across 2.000 watermarked images under the RGB salt & pepper noise ( $p = 0.03$ ) perturbation against unperturbed, unwatermarked images for different hashing prefixes on LlamaGen (GPT-L) using  $k = 8$  clusters, penalty  $\delta = 5$  and green token fraction  $\gamma = 0.5$ .

hash prefixes and showing the histograms of green token counts. It can be observed that some prefixes yield clearly separable data, while others lead to significant overlap.

However, since the service provider has control over the prefix, this variance can be used as an opportunity to improve watermark detection robustness. The service provider can run an evaluation over several prefixes, and use the best ones in deployment. The prefixes chosen for the main table are determined by averaging all TPR values and choosing the best performing prefix.

## 5. Related Work

The integration of watermarks into AI-generated images can be realized in different ways. Post-processing techniques [1, 8, 18, 25, 40, 42] apply watermarking to existing images in a post-hoc manner. Another possibility is to integrate watermarking directly during the generation process. Various techniques have been proposed here for large-scale text-to-image diffusion models [5, 7, 10, 31, 36]. For instance, the decoder of a latent diffusion model (LDM) can be finetuned to always create watermarked images from the latents [6, 10, 34]. Alternatively, inversion-based semantic watermarking modifies the initial latent noise during generation to contain a pattern, which is recoverable through the inversion of the denoising process [7, 11, 31, 36]. Since only the initial latent is modified, the watermark becomes an inherent part of the generated image. The diffusion model is

not changed. Semantic watermarking thus makes use of the many different ways to create an image that fulfills the user specifications (e.g. the prompt). In this work, we also aim to integrate watermarking during generation by proposing a concept for AR image generation where the token sampling is biased.

Concurrently to our work, some recently released preprints have also investigated token-level watermarking for AR image models [13, 28, 33]. To the best of our knowledge, our work and the aforementioned concurrent works are the first research efforts to examine red-green watermarking for discrete token-based AR models for image generation. Wu et al. [33] propose a different clustering-based approach evaluated on a different model (Emu-3), and only provides a very limited robustness study by evaluating robustness to  $l_2$  and  $l_\infty$  noise. Tong et al. [28] computes pairs of similar tokens but instead of assigning the same color to similar tokens, assigns one token in the pair to the green set and the other one to the red set. They also train an index reconstruction model to improve token reconstruction accuracy. Similar to Tong et al. [28], Jovanović et al. [13] train a token reconstruction model. However, they also consider perturbations during training to improve the robustness of the red-green watermarking. In contrast, our base clustering approach is training-free, simple to use, and already provides high robustness and image quality. Our cluster classifier is similar in spirit to the trained token reconstructors of Tong et al. [28] and Jovanović et al. [13], with the difference that we directly predict the clusters. Moreover, the method described by Jovanović et al. [13] also requires finetuning the VAE decoder, which complicates the training process and requires an additional image reconstruction loss.

Related to our cluster-based red-green watermarking are semantic watermarking methods for LLMs (e.g., Ren et al. [21]), developed to resist synonym and paraphrasing attacks by grouping tokens with similar embeddings.

## 6. Conclusion

In this work, we have investigated clustering as a potential solution to the poor robustness of red-green watermarking in autoregressive models for image generation. A thorough study of this approach was presented, conducted on different models, where we explored the effect of various choices in an extensive ablation study. The results indicate that clustering can be effective in improving robustness. In fact, it significantly boosts watermark detection, except in the most challenging and destructive settings (salt-and-pepper noise, blurring). On top of just clustering, which is training-free, this work also investigates finetuning a cluster classifier, which further boosts robustness of cluster-based red-green watermarking, beating the available baselines. However, important avenues for future work remain. Like many recent watermarking methods for gen-

erative models of images [11, 31, 36], token-based watermarks cannot be robust to geometric transforms (rotation, zoom) because these transforms introduce spatial misalignment between patches responsible for the tokens before and after the transform. We believe this requires further research into synchronization. We hope our work serves as a strong foundation for future research on the robust detection of generated images. To support further developments in this field, we will make our code publicly available.

## References

- [1] Ali Al-Haj. Combined dwt-dct digital image watermarking. *Journal of computer science*, 3(9):740–746, 2007. [5](#) [7](#)
- [2] Huiwen Chang, Han Zhang, Lu Jiang, Ce Liu, and William T. Freeman. Maskgit: Masked generative image transformer. In *Proc. of IEEE Conference on Computer Vision and Pattern Recognition (CVPR)*, pages 11315–11325, June 2022. [1](#) [2](#)
- [3] Huiwen Chang, Han Zhang, Jarred Barber, Aaron Maschinot, Jose Lezama, Lu Jiang, Ming-Hsuan Yang, Kevin Patrick Murphy, William T. Freeman, Michael Rubinstein, Yuanzhen Li, and Dilip Krishnan. Muse: Text-to-image generation via masked generative transformers. In Andreas Krause, Emma Brunskill, Kyunghyun Cho, Barbara Engelhardt, Sivan Sabato, and Jonathan Scarlett, editors, *Proc. of Int. Conference on Machine Learning (ICML)*, volume 202 of *Proceedings of Machine Learning Research*, pages 4055–4075. PMLR, 23–29 Jul 2023. [1](#) [2](#)
- [4] Miranda Christ, Sam Gunn, and Or Zamir. Undetectable watermarks for language models. In *Proc. of the Annual ACM Workshop on Computational Learning Theory (COLT)*, volume 210 of *Proceedings of Machine Learning Research*, pages 1125–1139. PMLR, 2024. URL <https://proceedings.mlr.press/v210/christ24a.html>. [2](#)
- [5] Hai Ci, Yiren Song, Pei Yang, Jinheng Xie, and Mike Zheng Shou. WMAdapter: Adding watermark control to latent diffusion models, 2024. [7](#)
- [6] Hai Ci, Yiren Song, Pei Yang, Jinheng Xie, and Mike Zheng Shou. WMAdapter: Adding watermark control to latent diffusion models, 2024. [7](#)
- [7] Hai Ci, Pei Yang, Yiren Song, and Mike Zheng Shou. RingID: Rethinking tree-ring watermarking for enhanced multi-key identification. In Aleš Leonardis, Elisa Ricci, Stefan Roth, Olga Russakovsky, Torsten Sattler, and Gü̈l Varol, editors, *Proc. of the European Conference on Computer Vision (ECCV)*, pages 338–354, Cham, 2024. Springer Nature Switzerland. ISBN 978-3-031-73390-1. [7](#)
- [8] Ingemar Cox, Matthew Miller, Jeffrey Bloom, Jessica Fridrich, and Ton Kalker. *Digital Watermarking and Steganography*. Morgan Kaufmann Publishers Inc., San Francisco, CA, USA, 2 edition, 2007. [7](#)
- [9] Lijie Fan, Tianhong Li, Siyang Qin, Yuanzhen Li, Chen Sun, Michael Rubinstein, Deqing Sun, Kaiming He, and Yonglong Tian. Fluid: Scaling autoregressive text-to-image generative models with continuous tokens. In *International Conference on Learning Representations (ICLR)*, 2025. [1](#) [2](#)
- [10] Pierre Fernandez, Guillaume Couairon, Hervé Jégou, Matthijs Douze, and Teddy Furon. The stable signature: Rooting watermarks in latent diffusion models. In *Proc. of IEEE Conference on Computer Vision and Pattern Recognition (CVPR)*, 2023. [1](#) [7](#)
- [11] Sam Gunn, Xuandong Zhao, and Dawn Song. An undetectable watermark for generative image models. In *International Conference on Learning Representations (ICLR)*, 2025. [7](#) [8](#)
- [12] Martin Heusel, Hubert Ramsauer, Thomas Unterthiner, Bernhard Nessler, and Sepp Hochreiter. Gans trained by a two time-scale update rule converge to a local nash equilibrium. In I. Guyon, U. Von Luxburg, S. Bengio, H. Wallach, R. Fergus, S. Vishwanathan, and R. Garnett, editors, *Advances in Neural Information Processing Systems (NIPS)*, volume 30, 2017. [5](#)
- [13] Nikola Jovanović, Ismail Labiad, Tomáš Souček, Martin Vechev, and Pierre Fernandez. Watermarking autoregressive image generation, 2025. [8](#)
- [14] John Kirchenbauer, Jonas Geiping, Yuxin Wen, Jonathan Katz, Ian Miers, and Tom Goldstein. A watermark for large language models. In *Proc. of Int. Conference on Machine Learning (ICML)*, pages 17061–17084. PMLR, 2023. [1](#) [2](#)
- [15] John Kirchenbauer, Jonas Geiping, Yuxin Wen, Manli Shu, Khalid Saifullah, Kezhi Kong, Kasun Fernando, Aniruddha Saha, Micah Goldblum, and Tom Goldstein. On the reliability of watermarks for large language models. In *International Conference on Learning Representations (ICLR)*, 2024. [2](#)
- [16] Rohith Kuditipudi, John Thickstun, Tatsunori Hashimoto, and Percy Liang. Robust distortion-free watermarks for language models. *Transactions on Machine Learning Research (TMLR)*, 2024. [2](#)
- [17] Hermann Kumbong, Xian Liu, Tsung-Yi Lin, Ming-Yu Liu, Xihui Liu, Ziwei Liu, Daniel Y. Fu, Christopher Re, and David W. Romero. Hmar: Efficient hierarchical masked auto-regressive image generation. In *Proc. of IEEE Conference on Computer Vision and Pattern Recognition (CVPR)*, pages 2535–2544, June 2025. [1](#) [2](#)
- [18] Shilin Lu, Zihan Zhou, Jiayou Lu, Yuanzhi Zhu, and Adams Wai-Kin Kong. Robust watermarking using generative priors against image editing: From benchmarking to advances. In *International Conference on Learning Representations (ICLR)*, 2025. URL <https://openreview.net/forum?id=1608GCm8Wn>. [7](#)
- [19] Nahema Marchal, Rachel Xu, Rasmi Elasmar, Iason Gabriel, Beth Goldberg, and William Isaac. Generative ai misuse: A taxonomy of tactics and insights from real-world data, 2024. [1](#)
- [20] K. A. Navas, Mathews Cherian Ajay, M. Lekshmi, Tamby S. Archana, and M. Sasikumar. Dwt-dct-svd based watermarking. In *2008 3rd International Conference on Communication Systems Software and Middleware and Workshops (COMSWARE '08)*, pages 271–274, 2008. doi: 10.1109/COMSWA.2008.4554423. [5](#)

[21] Jie Ren, Han Xu, Yiding Liu, Yingqian Cui, Shuaiqiang Wang, Dawei Yin, and Jiliang Tang. A robust semantics-based watermark for large language model against paraphrasing. In *Findings of the Association for Computational Linguistics: NAACL*, pages 613–625, 2024. 2, 8

[22] Robin Rombach, Andreas Blattmann, Dominik Lorenz, Patrick Esser, and Björn Ommer. High-resolution image synthesis with latent diffusion models. In *Proc. of IEEE Conference on Computer Vision and Pattern Recognition (CVPR)*, pages 10684–10695, June 2022. 5, 11

[23] Olga Russakovsky, Jia Deng, Hao Su, Jonathan Krause, Sanjeev Satheesh, Sean Ma, Zhiheng Huang, Andrej Karpathy, Aditya Khosla, Michael Bernstein, Alexander C. Berg, and Li Fei-Fei. ImageNet large scale visual recognition challenge. *International Journal of Computer Vision (IJCV)*, 115(3):211–252, 2015. doi: 10.1007/s11263-015-0816-y. 4

[24] Peize Sun, Yi Jiang, Shoufa Chen, Shilong Zhang, Bingyue Peng, Ping Luo, and Zehuan Yuan. Autoregressive model beats diffusion: Llama for scalable image generation, 2024. 1, 2, 4

[25] Matthew Tancik, Ben Mildenhall, and Ren Ng. Stegastamp: Invisible hyperlinks in physical photographs. In *Proc. of IEEE Conference on Computer Vision and Pattern Recognition (CVPR)*, pages 2117–2126, 2020. 7

[26] Haotian Tang, Yecheng Wu, Shang Yang, Enze Xie, Junsong Chen, Junyu Chen, Zhuoyang Zhang, Han Cai, Yao Lu, and Song Han. HART: Efficient visual generation with hybrid autoregressive transformer. In *International Conference on Learning Representations (ICLR)*, 2025. 1, 2

[27] Keyu Tian, Yi Jiang, Zehuan Yuan, BINGYUE PENG, and Liwei Wang. Visual autoregressive modeling: Scalable image generation via next-scale prediction. In *Advances in Neural Information Processing Systems (NeurIPS)*, 2024. 1, 2

[28] Yu Tong, Zihao Pan, Shuai Yang, and Kaiyang Zhou. Training-free watermarking for autoregressive image generation, 2025. 5, 8, 11

[29] Xinlong Wang, Xiaosong Zhang, Zhengxiong Luo, Quan Sun, Yufeng Cui, Jinsheng Wang, Fan Zhang, Yueze Wang, Zhen Li, Qiyi Yu, Yingli Zhao, Yulong Ao, Xuebin Min, Tao Li, Boya Wu, Bo Zhao, Bowen Zhang, Liangdong Wang, Guang Liu, Zheqi He, Xi Yang, Jingjing Liu, Yonghua Lin, Tiejun Huang, and Zhongyuan Wang. Emu3: Next-token prediction is all you need, 2024. 1, 2

[30] Yuqing Wang, Zhijie Lin, Yao Teng, Yuanzhi Zhu, Shuhuai Ren, Jiashi Feng, and Xihui Liu. Bridging continuous and discrete tokens for autoregressive visual generation. In *Proc. of the IEEE/CVF International Conference on Computer Vision (ICCV)*, 2025. 1, 2

[31] Yuxin Wen, John Kirchenbauer, Jonas Geiping, and Tom Goldstein. Tree-Ring watermarks: Invisible fingerprints for diffusion images. In *Advances in Neural Information Processing Systems (NeurIPS)*, 2023. 1, 6, 7, 8

[32] Yihan Wu, Zhengmian Hu, Junfeng Guo, Hongyang Zhang, and Heng Huang. A resilient and accessible distribution-preserving watermark for large language models. In *Proc. of Int. Conference on Machine Learning (ICML)*, pages 53443–53470. PMLR, 2024. 2

[33] Yihan Wu, Xuehao Cui, Ruibo Chen, Georgios Milis, and Heng Huang. A watermark for auto-regressive image generation models, 2025. 8

[34] Cheng Xiong, Chuan Qin, Guorui Feng, and Xinpeng Zhang. Flexible and secure watermarking for latent diffusion model. In *Proc. ACM Internation Conference on Multimedia (ACM MM)*, MM '23, page 1668–1676, New York, NY, USA, 2023. Association for Computing Machinery. ISBN 9798400701085. doi: 10.1145/3581783.3612448. 7

[35] Zhiyuan Yan, Junyan Ye, Weijia Li, Zilong Huang, Shenghai Yuan, Xiangyang He, Kaiqing Lin, Jun He, Conghui He, and Li Yuan. Gpt-imgeval: A comprehensive benchmark for diagnosing gpt4o in image generation, 2025. 1

[36] Zijin Yang, Kai Zeng, Kejiang Chen, Han Fang, Weiming Zhang, and Nenghai Yu. Gaussian Shading: Provable performance-lossless image watermarking for diffusion models. In *Proc. of IEEE Conference on Computer Vision and Pattern Recognition (CVPR)*, 2024. 1, 7, 8

[37] KiYoon Yoo, Wonhyuk Ahn, Jiho Jang, and Nojun Kwak. Robust multi-bit natural language watermarking through invariant features. In *Proc. of the Annual Meeting of the Association for Computational Linguistics (ACL)*, pages 2092–2115, 2023. 2

[38] Jiahui Yu, Yuanzhong Xu, Jing Yu Koh, Thang Luong, Gunnar Baid, Zirui Wang, Vijay Vasudevan, Alexander Ku, Yinfei Yang, Burcu Karagol Ayan, Ben Hutchinson, Wei Han, Zarana Parekh, Xin Li, Han Zhang, Jason Baldridge, and Yonghui Wu. Scaling autoregressive models for content-rich text-to-image generation. *Transactions on Machine Learning Research*, 2022. ISSN 2835-8856. 1, 2

[39] Qihang Yu, Ju He, Xueqing Deng, Xiaohui Shen, and Liang-Chieh Chen. Randomized autoregressive visual generation, 2024. 1, 2, 4

[40] Kevin Alex Zhang, Lei Xu, Alfredo Cuesta-Infante, and Kalyan Veeramachaneni. Robust invisible video watermarking with attention, 2019. 5, 7

[41] Xuandong Zhao, Kexun Zhang, Zihao Su, Saastha Vasan, Ilya Grishchenko, Christopher Kruegel, Giovanni Vigna, Yu-Xiang Wang, and Lei Li. Invisible image watermarks are provably removable using generative AI. In *Advances in Neural Information Processing Systems (NeurIPS)*, 2024. URL <https://openreview.net/forum?id=7hy5fy2OC6>. 5, 11

[42] Jiren Zhu, Russell Kaplan, Justin Johnson, and Li Fei-Fei. Hidden: Hiding data with deep networks. In *Proc. of the European Conference on Computer Vision (ECCV)*, pages 657–672, 2018. 7

## A. Full Experimental Setup and Results

### A.1. Image Generation Settings

Table 3 shows detailed generation settings for the models (*LlamaGen*<sup>2</sup> and *RAR*<sup>3</sup>) used in this paper.

	LlamaGen (GPT-B)	LlamaGen (GPT-L)	RAR-XL
Resolution	256 × 256	384 × 384	256 × 256
$ \mathbb{V} $	16384	16384	1024
CFG scale	2.0	2.0	6.9
CFG pow	–	–	1.5
top-k	$ \mathbb{V} $	$ \mathbb{V} $	$ \mathbb{V} $
top-p	1.0	1.0	1.0
temperature	1.0	1.0	1.02

Table 3. Model and generation details.

### A.2. Baseline Settings

Baseline methods (*DWT-DCT*, *DWT-DCT-SVD*, and *RivaGAN*) are taken from a commonly used implementation of post-hoc watermarking schemes<sup>4</sup>. For DWT-DCT as well as DWT-DCT-SVD, we encode 64 random bits for each image. For RivaGAN, we randomly encode 32 bits as this is the maximum supported by the implementation. Detection is done by extracting bits from images and assessing the ratio of matching bits. For *IndexMark* [28], we use their official implementation<sup>5</sup>. Similar to our main methods, AUC and TPR are determined empirically by calculating ROC.

### A.3. Visual Examples of Perturbations

Figure 6 shows the perturbations applied during all experiments. *Brightness*, *Contrast*, *hue*, and *saturation* are summarized as *jitter*. Results for *SD1.5-AE*, *FLUX.1-AE* and *SD2.1 Regeneration* are averaged and summarized as *regeneration*. The regeneration attack [41] is performed with default settings<sup>6</sup>, i.e. 60 steps of denoising using Stable Diffusion 2.1 [22].

### A.4. Perturbation Sets

We use two perturbations sets for evaluation throughout the paper. *Perturbation Set A* is defined in Table 4, and *Perturbation Set 2* is defined in Table 5. The latter has much stronger perturbations. Table 6 shows the perturbation settings used during training of the cluster classifier. Note that for the color jitter perturbations, values are sampled randomly in the range specified by maximum intensity given in the tables. The specific implementations of each perturbation can be found in our project repository.

<sup>2</sup><https://github.com/FoundationVision/LlamaGen>

<sup>3</sup><https://github.com/bytedance/ld-tokenizer>

<sup>4</sup><https://github.com/ShieldMnt/invisible-watermark>

<sup>5</sup><https://github.com/maifoundations/IndexMark>

<sup>6</sup><https://github.com/XuandongZhao/WatermarkAttacker>

Augmentation Type	Parameter(s)
Gaussian noise	$\sigma = 0.05$
JPEG compression	Quality = 60
Gaussian blur	$r = 2$
RGB salt & pepper noise	$p = 0.03$
Random Drop	Ratio = 0.3
Brightness jitter	Max. Intensity = 3
Contrast jitter	Max. Intensity = 1.5
Hue jitter	Max. Intensity = 0.1
Saturation jitter	Max. Intensity = 2
SD1.5-AE	–
FLUX.1-AE	–
SD2.1-Regeneration	60 Denoising Steps

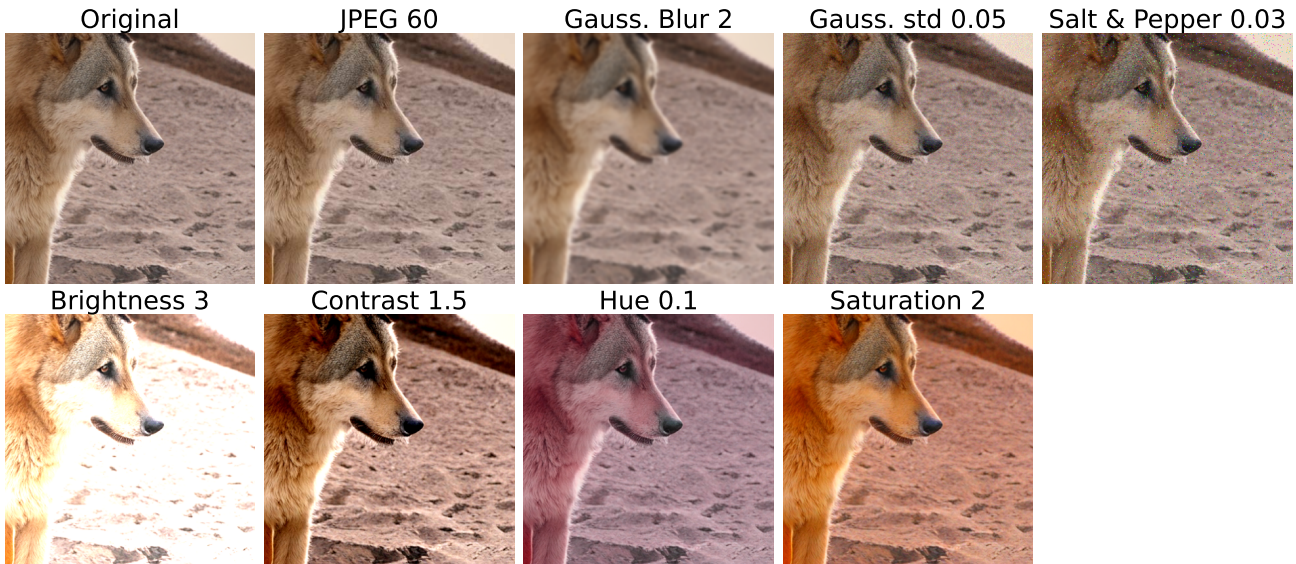
Table 4. **Perturbations set A**: This set is used in the ablation study and for prefix tuning.

Augmentation Type	Parameter(s)
Gaussian noise	$\sigma = 0.2$
JPEG compression	Quality = 20
Gaussian blur	$r = 3$
RGB salt & pepper noise	$p = 0.1$
Random Drop	Ratio = 0.5
Brightness jitter	Max. Intensity = 4
Contrast jitter	Max. Intensity = 4
Hue jitter	Max. Intensity = 0.5
Saturation jitter	Max. Intensity = 5
SD1.5-AE	–
FLUX.1-AE	–
SD2.1-Regeneration	60 Denoising Steps

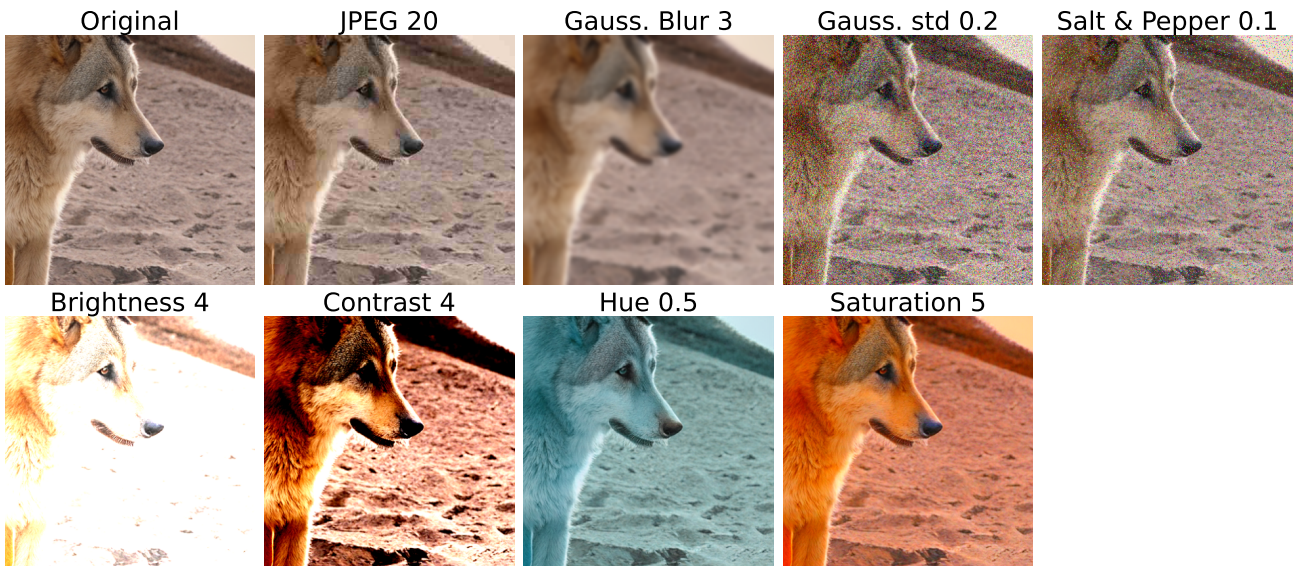
Table 5. **Perturbation set B**: This more challenging set is used for the main results in Table 1

Augmentation Type	Parameter(s)
Gaussian noise	$\sigma = 0.1$
JPEG compression	Quality range: 80 – 20
Gaussian blur	Max radius = 2
RGB salt & pepper noise	Max $p = 0.07$
Brightness jitter	Max intensity = 4
Contrast jitter	Max intensity = 2
Hue jitter	Max intensity = 0.1
Saturation jitter	Max intensity = 2

Table 6. Data augmentation settings and parameters used during training of the Cluster Classifier.



(a) Examples of **Perturbation Set A** without regeneration attacks (default perturbations used for the ablation and prefix tuning.)



(b) Examples of **Perturbation Set B** without regeneration attacks (strong perturbations used for main results in Table 1)



(c) Regeneration attacks. SD1.5-AE and FLUX.1-AE show encode-decode attacks with their respective autoencoders. SD2.1-Regeneration shows the regeneration attack. These attacks are included in both **Perturbation Sets A and B**

Figure 6. Examples of visual perturbations.

## A.5. Computing Infrastructure and Software Details

The experiments were conducted on two servers.

- One Server with 4 Nvidia A40 GPUs, 64 AMD EPYC 7452 32-Core Processors, and 500 GB RAM, running Ubuntu 20.04.6 LTS
- One Server with 4 Nvidia A40 GPUs, 32 AMD EPYC 7282 16-Core Processors, and 500 GB RAM, running Ubuntu 20.04.6 LTS

The exact Python version and package requirements can be found in our project repository.

## A.6. Number of Samples Used in Experiments

The samples generated for each experiment are as follows:

For each of the three models, we first generated 2.000 unwatermarked samples to obtain negative class samples, adding up to 6.000 images. The baselines methods (DWT-DCT, DWT-DCT-SVD, and RivaGAN) were applied to these unwatermarked images to obtain positive samples.

For our watermarking method, we then generated 2.000 samples for each setting combination (number of clusters  $k \in [-128, 64, 32, 16, 8]$ , penalty  $\delta \in [2, 5]$ , and green token fraction  $\gamma \in [0.5, 0.25]$ ) which can be seen in Table 7. This yields 24 setting per model, totaling  $24 \times 2.000 \times 3 = 144.000$  images. This is done for eight different prefixes  $\forall \kappa \in \{1, \dots, 8\}$ , totaling  $144.000 \times 8 = 1.152.000$  images. We then calculated AUC and TPR@FPR=1% against the 2.000 unwatermarked images obtained earlier. With these results, we are then able to pick the best performing hash prefix  $\kappa$  across each in each group (i.e. the index is given defined by the model, method, number of clusters  $k$ , penalty  $\delta$  and green token fraction  $\gamma$ ).

To calculate FID scores against 50.000 images in the ImageNet dataset, 50.000 watermarked images are again generated using the best performing hash prefix  $\kappa$  for each of the 24 settings for each of the 3 models model, yielding  $50.000 \times 24 \times 3 = 3.600.000$  images.

This adds up to 4.758.000 images generated in total.

## B. Additional experimental results

We provide the full results on the experiments:

**(1) Full Ablation Plots:** In Figure 7, the full ablation is provided for the effect of different watermarking settings on the FID. Figure 8 shows full ablation plots for different perturbations on how watermark detection performs under different watermarking settings.

**(2) Full Results Tables:** In Table 7, we provide full results on Perturbation Set A. The column  $\kappa$  shows the best performing hash prefix for each setting (Model, Method,  $k$ ,  $\delta$ ,  $\gamma$ ). Furthermore, Table 9 and Table 8 show mean and  $\sigma$  across different hash prefixes  $\kappa$  in terms of AUC and TPR@FPR=1%, respectively.

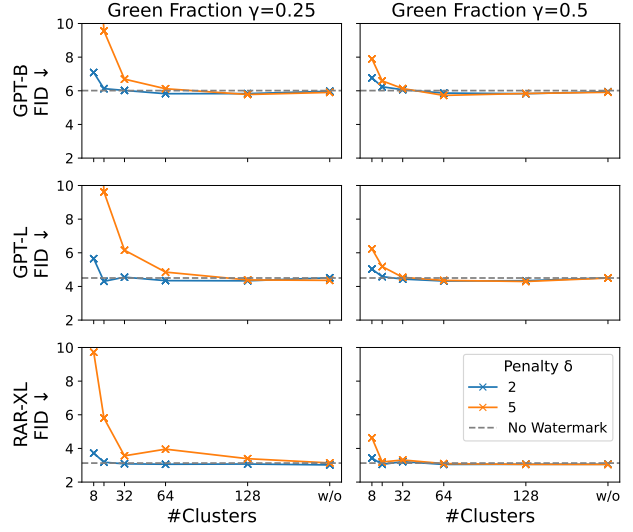


Figure 7. FIDs across models, amount of clusters, penalty  $\delta$ , and green fraction  $\gamma$  settings.

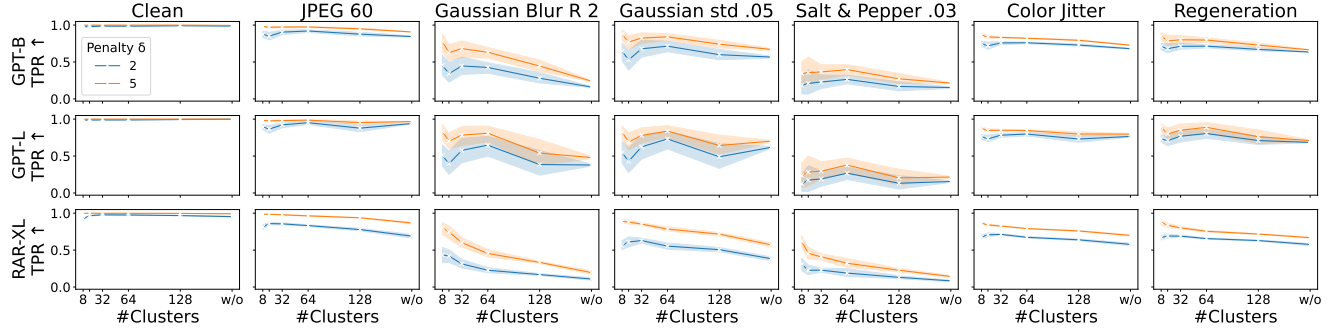
## C. Examples of Generated Images

In Figures 9 to 11, visual examples for both unwatermarked and watermarked images are shown for all models. For watermarked images, we set penalty  $\delta = 5$  and green token fraction  $\gamma = 0.25$ . We further show both images generated without clustering ( $k = 16384$  for LlamaGen GPT-B and GPT-L,  $k = 1024$  for RAR-XL), and clustering with  $k \in [128, 64, 8]$ . While watermarked images retain image quality down to  $k = 64$ , for the extreme case of  $k = 8$  there is decline in image quality.

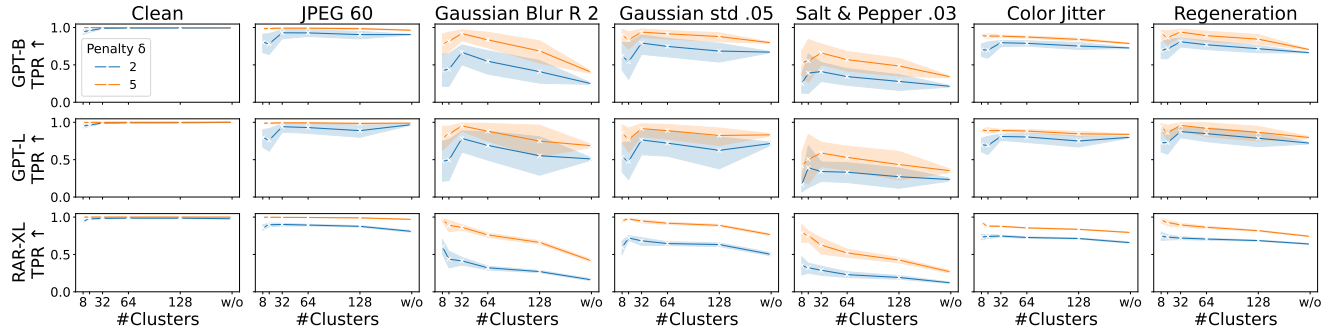
Model	Method	$k$	$\delta$	$\gamma$	$\kappa$	FID $\downarrow$	Clean	JPEG 60	Gauss. Blur R 2	Gauss. std. 0.05	Salt&Pepper .03	Color Jitter	Regeneration	Average		
GPT-B	No WM	-	-	-	-	6.01	-	-	-	-	-	-	-	-		
	DWT-DCT	-	-	-	-	6.02	0.960 — 0.837	0.511 — 0.015	0.535 — 0.028	0.939 — 0.712	0.929 — 0.564	0.673 — 0.388	0.519 — 0.016	0.708 — 0.349		
	DWT-DCT-SVD	-	-	-	-	6.51	1.000 — 1.000	0.993 — 0.947	0.997 — 0.980	0.991 — 0.981	0.902 — 0.359	0.601 — 0.287	0.826 — 0.494	0.857 — 0.652		
	RivaGAN	-	-	-	-	6.34	1.000 — 0.999	0.998 — 0.975	0.999 — 0.995	1.000 — 0.996	0.997 — 0.970	0.984 — 0.934	0.853 — 0.475	0.974 — 0.898		
Ours (No Clustering)	-	2	0.50	6	5.95	0.998 — 0.989	0.972 — 0.850	0.739 — 0.173	0.898 — 0.582	0.690 — 0.161	0.896 — 0.696	0.870 — 0.640	0.849 — 0.554	nan — nan		
	-	0.25	6	5.97	1.000 — 0.997	0.987 — 0.909	0.771 — 0.257	0.920 — 0.679	0.731 — 0.237	0.914 — 0.738	0.879 — 0.661	0.871 — 0.608				
	-	5	0.50	4	5.91	0.999 — 0.996	0.984 — 0.913	0.780 — 0.256	0.926 — 0.688	0.736 — 0.229	0.906 — 0.731	0.886 — 0.668	0.870 — 0.606			
	-	0.25	4	5.90	0.999 — 0.996	0.995 — 0.967	0.844 — 0.426	0.954 — 0.799	0.783 — 0.356	0.923 — 0.794	0.916 — 0.710	0.898 — 0.686				
	+ Clustering	8	2	0.50	4	6.77	0.990 — 0.972	0.987 — 0.942	0.949 — 0.657	0.972 — 0.848	0.953 — 0.558	0.898 — 0.768	0.974 — 0.815	0.922 — 0.739		
	-	0.25	5	7.09	0.995 — 0.981	0.992 — 0.966	0.974 — 0.794	0.975 — 0.874	0.932 — 0.521	0.939 — 0.825	0.986 — 0.880	0.948 — 0.790				
	-	5	0.50	4	7.90	0.998 — 0.995	0.999 — 0.993	0.989 — 0.914	0.993 — 0.985	0.982 — 0.741	0.924 — 0.839	0.995 — 0.945	0.949 — 0.854			
	-	0.25	5	18.91	1.000 — 0.999	0.999 — 0.999	0.998 — 0.985	0.998 — 0.983	0.987 — 0.869	0.977 — 0.928	0.999 — 0.995	0.984 — 0.936				
	-	16	2	0.50	2	6.24	0.991 — 0.978	0.987 — 0.944	0.944 — 0.673	0.949 — 0.741	0.982 — 0.720	0.931 — 0.811	0.975 — 0.824	0.944 — 0.775		
	-	0.25	2	6.13	0.997 — 0.987	0.991 — 0.965	0.924 — 0.655	0.979 — 0.894	0.995 — 0.942	0.946 — 0.857	0.983 — 0.910	0.957 — 0.852				
+ CC	-	5	0.50	2	6.59	1.000 — 0.998	0.998 — 0.988	0.980 — 0.878	0.980 — 0.881	0.991 — 0.864	0.955 — 0.879	0.996 — 0.946	0.968 — 0.882			
	-	0.25	6	9.56	1.000 — 1.000	1.000 — 0.998	0.996 — 0.967	0.999 — 0.996	0.996 — 0.976	0.982 — 0.947	1.000 — 0.995	0.988 — 0.962				
	-	32	2	0.50	6	6.07	0.991 — 0.981	0.990 — 0.948	0.999 — 0.576	0.993 — 0.893	0.888 — 0.470	0.903 — 0.787	0.966 — 0.783	0.917 — 0.731		
	-	0.25	6	6.02	0.997 — 0.994	0.993 — 0.975	0.949 — 0.722	0.993 — 0.947	0.942 — 0.679	0.942 — 0.845	0.984 — 0.889	0.953 — 0.825				
	-	5	0.50	6	6.13	1.000 — 0.999	0.998 — 0.985	0.967 — 0.795	0.997 — 0.956	0.929 — 0.609	0.932 — 0.848	0.991 — 0.890	0.946 — 0.822			
	-	0.25	6	6.69	1.000 — 1.000	0.999 — 0.996	0.994 — 0.961	0.999 — 0.996	0.984 — 0.903	0.975 — 0.925	0.999 — 0.988	0.983 — 0.939				
	-	64	2	0.50	3	5.86	0.993 — 0.982	0.988 — 0.940	0.888 — 0.482	0.979 — 0.825	0.837 — 0.364	0.908 — 0.777	0.958 — 0.751	0.907 — 0.690		
	-	0.25	7	5.83	0.998 — 0.994	0.995 — 0.980	0.949 — 0.744	0.977 — 0.871	0.901 — 0.515	0.931 — 0.827	0.980 — 0.852	0.939 — 0.784				
	-	5	0.50	3	5.73	1.000 — 0.999	0.998 — 0.982	0.949 — 0.685	0.990 — 0.916	0.890 — 0.493	0.927 — 0.828	0.983 — 0.856	0.935 — 0.777			
	-	0.25	7	6.12	1.000 — 1.000	1.000 — 0.999	0.992 — 0.956	0.996 — 0.974	0.951 — 0.731	0.958 — 0.894	0.997 — 0.972	0.969 — 0.897				
GPT-L	No WM	-	-	-	-	4.50	-	-	-	-	-	-	-	nan — nan		
	DWT-DCT	-	-	-	-	4.36	0.932 — 0.800	0.537 — 0.015	0.576 — 0.044	0.912 — 0.722	0.943 — 0.704	0.683 — 0.403	0.538 — 0.027	0.715 — 0.367		
	DWT-DCT-SVD	-	-	-	-	4.54	1.000 — 0.999	0.989 — 0.935	0.995 — 0.977	0.996 — 0.992	0.960 — 0.686	0.614 — 0.436	0.888 — 0.628	0.875 — 0.718		
	RivaGAN	-	-	-	-	4.62	1.000 — 0.999	1.000 — 0.993	1.000 — 0.998	1.000 — 0.998	0.998 — 0.997	0.989 — 0.953	0.910 — 0.596	0.984 — 0.924		
	Ours (No Clustering)	-	2	0.50	7	4.51	1.000 — 1.000	0.992 — 0.945	0.835 — 0.377	0.906 — 0.629	0.696 — 0.165	0.932 — 0.787	0.907 — 0.685	0.885 — 0.633		
	-	0.25	4	4.52	1.000 — 1.000	0.996 — 0.981	0.892 — 0.544	0.936 — 0.746	0.732 — 0.264	0.926 — 0.812	0.932 — 0.732	0.898 — 0.694				
	-	5	0.50	7	4.50	1.000 — 1.000	0.995 — 0.968	0.882 — 0.495	0.931 — 0.705	0.719 — 0.224	0.940 — 0.817	0.926 — 0.708	0.902 — 0.678			
	-	0.25	4	4.36	1.000 — 1.000	0.998 — 0.985	0.937 — 0.712	0.964 — 0.849	0.793 — 0.380	0.936 — 0.848	0.961 — 0.812	0.923 — 0.766				
	+ Clustering	8	2	0.50	4	5.03	0.988 — 0.969	0.987 — 0.957	0.959 — 0.835	0.836 — 0.863	0.953 — 0.555	0.892 — 0.790	0.977 — 0.905	0.920 — 0.783		
	-	0.25	5	5.65	0.995 — 0.980	0.995 — 0.973	0.981 — 0.894	0.972 — 0.848	0.908 — 0.394	0.941 — 0.838	0.989 — 0.932	0.947 — 0.796				
+ CC	-	5	0.50	4	6.24	0.999 — 0.998	0.999 — 0.997	0.996 — 0.983	0.992 — 0.952	0.984 — 0.754	0.918 — 0.851	0.997 — 0.988	0.946 — 0.873			
	-	0.25	5	22.08	1.000 — 1.000	1.000 — 1.000	0.999 — 0.995	0.999 — 0.991	0.977 — 0.773	0.980 — 0.935	0.999 — 0.988	0.984 — 0.931				
	-	16	2	0.50	2	4.58	0.992 — 0.978	0.988 — 0.952	0.948 — 0.780	0.940 — 0.708	0.988 — 0.787	0.930 — 0.830	0.980 — 0.894	0.945 — 0.809		
	-	0.25	2	4.30	0.996 — 0.990	0.993 — 0.973	0.951 — 0.802	0.973 — 0.890	0.999 — 0.983	0.948 — 0.882	0.988 — 0.951	0.965 — 0.892				
	-	5	0.50	2	5.18	1.000 — 1.000	0.999 — 0.994	0.987 — 0.949	0.976 — 0.874	0.994 — 0.894	0.953 — 0.893	0.997 — 0.983	0.968 — 0.906			
	-	0.25	8	9.62	1.000 — 1.000	1.000 — 1.000	0.996 — 0.983	0.991 — 0.998	0.999 — 0.998	0.981 — 0.981	0.986 — 0.967	1.000 — 0.999	0.991 — 0.977			
	-	32	2	0.50	6	4.44	0.991 — 0.984	0.993 — 0.979	0.950 — 0.828	0.996 — 0.952	0.877 — 0.477	0.905 — 0.835	0.982 — 0.906	0.922 — 0.805		
	-	0.25	6	4.55	0.999 — 0.994	0.997 — 0.985	0.976 — 0.898	0.996 — 0.962	0.949 — 0.692	0.943 — 0.870	0.994 — 0.962	0.959 — 0.871				
	-	5	0.50	6	4.54	1.000 — 1.000	0.999 — 0.994	0.989 — 0.953	0.998 — 0.985	0.920 — 0.624	0.929 — 0.880	0.999 — 0.978	0.946 — 0.872			
	-	0.25	6	6.15	1.000 — 1.000	0.999 — 0.994	0.998 — 0.990	0.999 — 0.993	0.983 — 0.894	0.974 — 0.940	1.000 — 0.998	0.983 — 0.952				
+ RAR-XL	No WM	-	-	-	-	3.13	-	-	-	-	-	-	-	nan — nan		
	DWT-DCT	-	-	-	-	3.29	0.976 — 0.883	0.526 — 0.013	0.539 — 0.027	0.947 — 0.741	0.938 — 0.579	0.696 — 0.432	0.534 — 0.013	0.721 — 0.369		
	DWT-DCT-SVD	-	-	-	-	3.87	1.000 — 1.000	0.996 — 0.949	0.999 — 0.986	0.998 — 0.990	0.909 — 0.306	0.606 — 0.273	0.819 — 0.462	0.860 — 0.641		
	RivaGAN	-	-	-	-	3.64	1.000 — 1.000	0.999 — 0.993	1.000 — 0.997	1.000 — 0.999	0.998 — 0.977	0.989 — 0.947	0.870 — 0.496	0.979 — 0.909		
	Ours (No Clustering)	-	2	0.50	3	3.06	0.995 — 0.968	0.963 — 0.745	0.760 — 0.153	0.874 — 0.449	0.697 — 0.105	0.897 — 0.618	0.888 — 0.611	0.855 — 0.498		
	-	0.25	2	3.02	0.999 — 0.989	0.979 — 0.845	0.788 — 0.203	0.907 — 0.551	0.709 — 0.132	0.914 — 0.691	0.907 — 0.661	0.873 — 0.557				
	-	5	0.50	3	3.05	1.000 — 0.995	0.988 — 0.904	0.809 — 0.249	0.925 — 0.634	0.736 — 0.174	0.922 — 0.725	0.916 — 0.693	0.886 — 0.597			
	-	0.25	2	3.14	1.000 — 1.000	0.998 — 0.974	0.898 — 0.466	0.969 — 0.786	0.796 — 0.299	0.942 — 0.812	0.949 — 0.764	0.922 — 0.700				
	+ Clustering	8	2	0.50	2	3.43	0.997 — 0.958	0.990 — 0.887	0.931 — 0.447	0.969 — 0.721	0.931 — 0.480	0.955 — 0.734	0.966 — 0.716	0.955 — 0.676		
	-	0.25	2	3.72	0.997 — 0.957	0.994 — 0.917	0.980 — 0.754	0.967 — 0.716	0.948 — 0.626	0.966 — 0.791	0.983 — 0.814	0.971 — 0.771				
+ CC	-	5	0.50	8	4.63	1.000 — 0.995	0.998 — 0.975	0.998 — 0.961	0.977 — 0.875	0.950 — 0.705	0.970 — 0.692	0.984 — 0.998	0.948 — 0.975	0.986 — 0.868		
	-	0.25	2	9.72	1.000 — 1.000	1.000 — 1.000	1.000 — 0.994	0.999 — 0.980	0.998 — 0.991	0.987 — 0.955	1.000 — 0.993	0.997 — 0.982				
	-	16	2	0.50	1	3.05	0.999 — 0.980	0.990 — 0.900	0.952 — 0.585	0.976 — 0.752	0.916 — 0.411	0.965 — 0.789	0.961 — 0.753	0.961 — 0.718		
	-	0.25	1	3.18	0.999 — 0.986	0.991 — 0.916	0.913 — 0.482	0.977 — 0.789	0.881 — 0.404	0.960 — 0.798	0.971 — 0.802	0.949 — 0.713				
	-	5	0.50	1	3.19	1.000 — 1.000	1.000 — 0.992	0.991 — 0.888	0.995 — 0.944	0.964 —						

Model	Method	k	$\delta$	$\gamma$	Clean	JPEG 60	Gauss. Blur R 2	Gauss. std. 05	Salt&Pepper .03	Color Jitter	Regeneration
GPT-B	No Clustering	-	2	0.50	0.988 $\pm$ 0.002	0.844 $\pm$ 0.013	0.161 $\pm$ 0.012	0.567 $\pm$ 0.022	0.154 $\pm$ 0.017	0.680 $\pm$ 0.009	0.634 $\pm$ 0.007
			0.25	0.995 $\pm$ 0.002	0.906 $\pm$ 0.005	0.248 $\pm$ 0.014	0.671 $\pm$ 0.011	0.212 $\pm$ 0.014	0.726 $\pm$ 0.010	0.662 $\pm$ 0.004	
		5	0.50	0.995 $\pm$ 0.001	0.907 $\pm$ 0.005	0.241 $\pm$ 0.012	0.670 $\pm$ 0.020	0.214 $\pm$ 0.013	0.727 $\pm$ 0.006	0.663 $\pm$ 0.006	
			0.25	0.998 $\pm$ 0.001	0.964 $\pm$ 0.005	0.401 $\pm$ 0.025	0.796 $\pm$ 0.013	0.339 $\pm$ 0.019	0.785 $\pm$ 0.010	0.703 $\pm$ 0.005	
	+ Clustering	8	2	0.50	0.979 $\pm$ 0.009	0.875 $\pm$ 0.065	0.456 $\pm$ 0.210	0.646 $\pm$ 0.181	0.183 $\pm$ 0.193	0.748 $\pm$ 0.055	0.709 $\pm$ 0.070
			0.25	0.943 $\pm$ 0.055	0.802 $\pm$ 0.192	0.428 $\pm$ 0.328	0.621 $\pm$ 0.283	0.250 $\pm$ 0.200	0.703 $\pm$ 0.131	0.694 $\pm$ 0.171	
		5	0.50	0.998 $\pm$ 0.002	0.981 $\pm$ 0.013	0.777 $\pm$ 0.186	0.876 $\pm$ 0.106	0.344 $\pm$ 0.249	0.864 $\pm$ 0.034	0.853 $\pm$ 0.069	
			0.25	0.999 $\pm$ 0.001	0.987 $\pm$ 0.014	0.782 $\pm$ 0.235	0.897 $\pm$ 0.131	0.535 $\pm$ 0.257	0.891 $\pm$ 0.021	0.912 $\pm$ 0.089	
		16	2	0.50	0.978 $\pm$ 0.010	0.851 $\pm$ 0.081	0.343 $\pm$ 0.200	0.529 $\pm$ 0.216	0.211 $\pm$ 0.259	0.721 $\pm$ 0.073	0.681 $\pm$ 0.092
			0.25	0.959 $\pm$ 0.037	0.783 $\pm$ 0.211	0.440 $\pm$ 0.330	0.542 $\pm$ 0.378	0.391 $\pm$ 0.417	0.698 $\pm$ 0.162	0.715 $\pm$ 0.196	
		32	5	0.50	0.998 $\pm$ 0.001	0.971 $\pm$ 0.018	0.628 $\pm$ 0.168	0.770 $\pm$ 0.140	0.355 $\pm$ 0.292	0.839 $\pm$ 0.034	0.785 $\pm$ 0.102
			0.25	0.999 $\pm$ 0.000	0.988 $\pm$ 0.013	0.817 $\pm$ 0.201	0.836 $\pm$ 0.181	0.552 $\pm$ 0.435	0.886 $\pm$ 0.045	0.866 $\pm$ 0.137	
		64	2	0.50	0.986 $\pm$ 0.008	0.905 $\pm$ 0.048	0.447 $\pm$ 0.184	0.679 $\pm$ 0.183	0.229 $\pm$ 0.147	0.758 $\pm$ 0.030	0.713 $\pm$ 0.062
			0.25	0.989 $\pm$ 0.007	0.929 $\pm$ 0.113	0.668 $\pm$ 0.229	0.792 $\pm$ 0.223	0.410 $\pm$ 0.205	0.797 $\pm$ 0.071	0.809 $\pm$ 0.097	
		128	5	0.50	0.999 $\pm$ 0.001	0.974 $\pm$ 0.017	0.681 $\pm$ 0.176	0.824 $\pm$ 0.113	0.366 $\pm$ 0.155	0.833 $\pm$ 0.016	0.801 $\pm$ 0.086
			0.25	0.999 $\pm$ 0.001	0.991 $\pm$ 0.015	0.919 $\pm$ 0.133	0.938 $\pm$ 0.092	0.659 $\pm$ 0.226	0.885 $\pm$ 0.024	0.939 $\pm$ 0.096	
		256	2	0.50	0.986 $\pm$ 0.005	0.920 $\pm$ 0.020	0.426 $\pm$ 0.106	0.714 $\pm$ 0.110	0.265 $\pm$ 0.094	0.761 $\pm$ 0.019	0.715 $\pm$ 0.036
			0.25	0.993 $\pm$ 0.002	0.928 $\pm$ 0.074	0.548 $\pm$ 0.244	0.747 $\pm$ 0.195	0.343 $\pm$ 0.177	0.788 $\pm$ 0.061	0.769 $\pm$ 0.089	
		512	5	0.50	0.998 $\pm$ 0.002	0.974 $\pm$ 0.011	0.632 $\pm$ 0.113	0.841 $\pm$ 0.075	0.397 $\pm$ 0.111	0.822 $\pm$ 0.009	0.797 $\pm$ 0.052
			0.25	1.000 $\pm$ 0.000	0.991 $\pm$ 0.011	0.835 $\pm$ 0.177	0.916 $\pm$ 0.086	0.570 $\pm$ 0.194	0.873 $\pm$ 0.022	0.891 $\pm$ 0.104	
		1024	2	0.50	0.991 $\pm$ 0.004	0.877 $\pm$ 0.040	0.280 $\pm$ 0.107	0.599 $\pm$ 0.108	0.169 $\pm$ 0.088	0.730 $\pm$ 0.026	0.671 $\pm$ 0.034
			0.25	0.994 $\pm$ 0.004	0.905 $\pm$ 0.081	0.409 $\pm$ 0.228	0.685 $\pm$ 0.203	0.279 $\pm$ 0.169	0.753 $\pm$ 0.070	0.716 $\pm$ 0.077	
		2048	5	0.50	0.999 $\pm$ 0.001	0.949 $\pm$ 0.020	0.445 $\pm$ 0.120	0.741 $\pm$ 0.083	0.272 $\pm$ 0.103	0.794 $\pm$ 0.016	0.730 $\pm$ 0.050
			0.25	0.999 $\pm$ 0.000	0.985 $\pm$ 0.015	0.686 $\pm$ 0.227	0.879 $\pm$ 0.095	0.485 $\pm$ 0.187	0.841 $\pm$ 0.030	0.844 $\pm$ 0.102	
	4096	2	0.50	0.983 $\pm$ 0.006	0.768 $\pm$ 0.122	0.871 $\pm$ 0.081	0.897 $\pm$ 0.044	0.977 $\pm$ 0.006	0.921 $\pm$ 0.013	0.626 $\pm$ 0.072	
		0.25	0.983 $\pm$ 0.018	0.748 $\pm$ 0.255	0.840 $\pm$ 0.217	0.887 $\pm$ 0.134	0.974 $\pm$ 0.032	0.923 $\pm$ 0.062	0.645 $\pm$ 0.166		
	8192	5	0.50	0.999 $\pm$ 0.001	0.894 $\pm$ 0.072	0.971 $\pm$ 0.020	0.966 $\pm$ 0.016	0.998 $\pm$ 0.002	0.960 $\pm$ 0.007	0.728 $\pm$ 0.059	
		0.25	1.000 $\pm$ 0.000	0.936 $\pm$ 0.083	0.897 $\pm$ 0.020	0.987 $\pm$ 0.015	0.999 $\pm$ 0.001	0.978 $\pm$ 0.008	0.830 $\pm$ 0.117		
GPT-L	No Clustering	-	2	0.50	0.998 $\pm$ 0.001	0.941 $\pm$ 0.008	0.379 $\pm$ 0.022	0.618 $\pm$ 0.020	0.155 $\pm$ 0.017	0.766 $\pm$ 0.015	0.684 $\pm$ 0.006
			0.25	0.999 $\pm$ 0.001	0.969 $\pm$ 0.008	0.510 $\pm$ 0.026	0.717 $\pm$ 0.030	0.234 $\pm$ 0.028	0.800 $\pm$ 0.012	0.721 $\pm$ 0.016	
		5	0.50	1.000 $\pm$ 0.000	0.967 $\pm$ 0.003	0.480 $\pm$ 0.026	0.702 $\pm$ 0.021	0.215 $\pm$ 0.019	0.797 $\pm$ 0.013	0.710 $\pm$ 0.011	
			0.25	1.000 $\pm$ 0.000	0.989 $\pm$ 0.004	0.687 $\pm$ 0.030	0.832 $\pm$ 0.024	0.351 $\pm$ 0.033	0.838 $\pm$ 0.010	0.796 $\pm$ 0.021	
	+ Clustering	8	2	0.50	0.985 $\pm$ 0.015	0.894 $\pm$ 0.051	0.508 $\pm$ 0.231	0.548 $\pm$ 0.230	0.122 $\pm$ 0.192	0.763 $\pm$ 0.047	0.732 $\pm$ 0.079
			0.25	0.951 $\pm$ 0.030	0.792 $\pm$ 0.191	0.480 $\pm$ 0.386	0.531 $\pm$ 0.322	0.167 $\pm$ 0.163	0.699 $\pm$ 0.138	0.725 $\pm$ 0.193	
		16	5	0.50	0.999 $\pm$ 0.001	0.984 $\pm$ 0.013	0.831 $\pm$ 0.168	0.824 $\pm$ 0.137	0.234 $\pm$ 0.062	0.870 $\pm$ 0.032	0.891 $\pm$ 0.076
			0.25	0.999 $\pm$ 0.001	0.987 $\pm$ 0.013	0.797 $\pm$ 0.256	0.857 $\pm$ 0.178	0.417 $\pm$ 0.278	0.896 $\pm$ 0.023	0.936 $\pm$ 0.070	
		32	2	0.50	0.989 $\pm$ 0.007	0.866 $\pm$ 0.081	0.396 $\pm$ 0.248	0.428 $\pm$ 0.266	0.175 $\pm$ 0.289	0.733 $\pm$ 0.071	0.709 $\pm$ 0.116
			0.25	0.963 $\pm$ 0.030	0.761 $\pm$ 0.240	0.494 $\pm$ 0.402	0.478 $\pm$ 0.435	0.392 $\pm$ 0.428	0.691 $\pm$ 0.180	0.730 $\pm$ 0.230	
		64	5	0.50	1.000 $\pm$ 0.000	0.976 $\pm$ 0.017	0.701 $\pm$ 0.163	0.691 $\pm$ 0.176	0.283 $\pm$ 0.325	0.847 $\pm$ 0.032	0.799 $\pm$ 0.113
			0.25	1.000 $\pm$ 0.001	0.989 $\pm$ 0.013	0.841 $\pm$ 0.195	0.769 $\pm$ 0.246	0.505 $\pm$ 0.486	0.888 $\pm$ 0.056	0.862 $\pm$ 0.145	
		128	2	0.50	0.990 $\pm$ 0.009	0.922 $\pm$ 0.053	0.577 $\pm$ 0.264	0.624 $\pm$ 0.263	0.190 $\pm$ 0.166	0.783 $\pm$ 0.043	0.769 $\pm$ 0.115
			0.25	0.991 $\pm$ 0.003	0.941 $\pm$ 0.104	0.784 $\pm$ 0.254	0.764 $\pm$ 0.262	0.341 $\pm$ 0.202	0.810 $\pm$ 0.069	0.876 $\pm$ 0.114	
		256	5	0.50	0.999 $\pm$ 0.001	0.980 $\pm$ 0.016	0.783 $\pm$ 0.200	0.779 $\pm$ 0.169	0.296 $\pm$ 0.193	0.850 $\pm$ 0.022	0.850 $\pm$ 0.126
			0.25	1.000 $\pm$ 0.001	0.993 $\pm$ 0.014	0.952 $\pm$ 0.102	0.915 $\pm$ 0.148	0.588 $\pm$ 0.251	0.891 $\pm$ 0.025	0.958 $\pm$ 0.103	
		512	2	0.50	0.990 $\pm$ 0.005	0.952 $\pm$ 0.035	0.647 $\pm$ 0.210	0.732 $\pm$ 0.186	0.268 $\pm$ 0.138	0.798 $\pm$ 0.035	0.805 $\pm$ 0.092
			0.25	0.994 $\pm$ 0.003	0.930 $\pm$ 0.103	0.690 $\pm$ 0.337	0.721 $\pm$ 0.296	0.332 $\pm$ 0.208	0.804 $\pm$ 0.092	0.848 $\pm$ 0.140	
		1024	5	0.50	1.000 $\pm$ 0.001	0.986 $\pm$ 0.012	0.809 $\pm$ 0.169	0.838 $\pm$ 0.130	0.378 $\pm$ 0.161	0.845 $\pm$ 0.020	0.889 $\pm$ 0.111
			0.25	1.000 $\pm$ 0.000	0.993 $\pm$ 0.011	0.880 $\pm$ 0.193	0.889 $\pm$ 0.154	0.531 $\pm$ 0.247	0.883 $\pm$ 0.037	0.919 $\pm$ 0.136	
		2048	2	0.50	0.995 $\pm$ 0.004	0.878 $\pm$ 0.075	0.385 $\pm$ 0.265	0.490 $\pm$ 0.255	0.132 $\pm$ 0.150	0.731 $\pm$ 0.072	0.710 $\pm$ 0.098
			0.25	0.995 $\pm$ 0.006	0.889 $\pm$ 0.136	0.552 $\pm$ 0.366	0.625 $\pm$ 0.343	0.272 $\pm$ 0.218	0.750 $\pm$ 0.124	0.787 $\pm$ 0.156	
		4096	5	0.50	1.000 $\pm$ 0.000	0.953 $\pm$ 0.034	0.540 $\pm$ 0.261	0.643 $\pm$ 0.197	0.205 $\pm$ 0.181	0.799 $\pm$ 0.045	0.762 $\pm$ 0.130
			0.25	1.000 $\pm$ 0.000	0.985 $\pm$ 0.019	0.749 $\pm$ 0.301	0.824 $\pm$ 0.189	0.435 $\pm$ 0.277	0.846 $\pm$ 0.053	0.865 $\pm$ 0.162	
		8192	2	0.50	0.985 $\pm$ 0.006	0.781 $\pm$ 0.211	0.892 $\pm$ 0.121	0.887 $\pm$ 0.093	0.979 $\pm$ 0.005	0.925 $\pm$ 0.019	0.678 $\pm$ 0.142
			0.25	0.980 $\pm$ 0.022	0.730 $\pm$ 0.369	0.800 $\pm$ 0.320	0.834 $\pm$ 0.240	0.965 $\pm$ 0.047	0.906 $\pm$ 0.097	0.688 $\pm$ 0.287	
		16384	5	0.50	0.999 $\pm$ 0.001	0.900 $\pm$ 0.117	0.981 $\pm$ 0.024	0.965 $\pm$ 0.028	0.999 $\pm$ 0.001	0.961 $\pm$ 0.006	0.804 $\pm$ 0.12

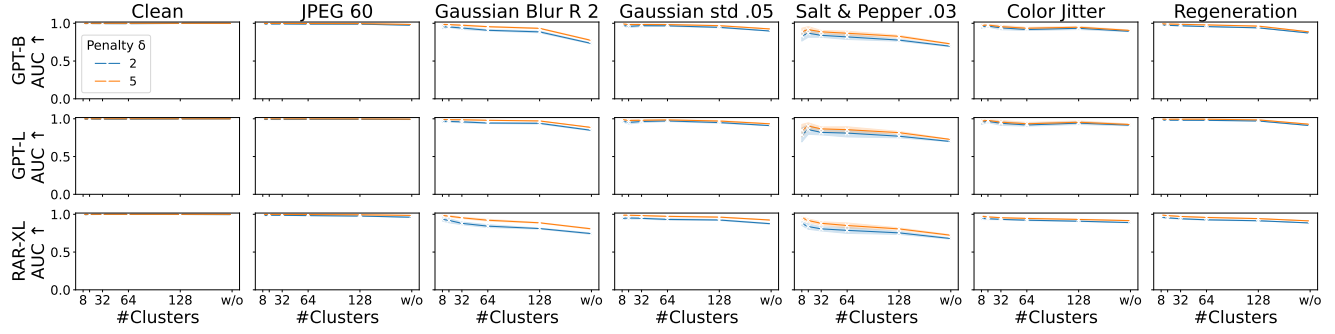
Model	Method	k	$\delta$	$\gamma$	Clean	JPEG 60	Gauss. Blur R 2	Gauss. std. 05	Salt&Pepper .03	Color Jitter	Regeneration		
GPT-B	No Clustering	-	2	0.50	0.998 $\pm$ 0.001	0.974 $\pm$ 0.003	0.732 $\pm$ 0.009	0.897 $\pm$ 0.004	0.695 $\pm$ 0.011	0.893 $\pm$ 0.008	0.869 $\pm$ 0.003		
			0.25	0.999 $\pm$ 0.001	0.985 $\pm$ 0.002	0.776 $\pm$ 0.007	0.922 $\pm$ 0.003	0.729 $\pm$ 0.006	0.903 $\pm$ 0.009	0.886 $\pm$ 0.003			
		5	0.50	0.999 $\pm$ 0.000	0.984 $\pm$ 0.001	0.772 $\pm$ 0.009	0.924 $\pm$ 0.004	0.726 $\pm$ 0.007	0.905 $\pm$ 0.007	0.885 $\pm$ 0.002			
			0.25	1.000 $\pm$ 0.001	0.994 $\pm$ 0.001	0.846 $\pm$ 0.005	0.954 $\pm$ 0.004	0.787 $\pm$ 0.007	0.920 $\pm$ 0.008	0.915 $\pm$ 0.002			
	+ Clustering	8	2	0.50	0.996 $\pm$ 0.004	0.991 $\pm$ 0.003	0.954 $\pm$ 0.035	0.975 $\pm$ 0.012	0.833 $\pm$ 0.102	0.956 $\pm$ 0.035	0.978 $\pm$ 0.004		
			0.25	0.995 $\pm$ 0.001	0.990 $\pm$ 0.004	0.959 $\pm$ 0.017	0.976 $\pm$ 0.011	0.911 $\pm$ 0.037	0.955 $\pm$ 0.019	0.981 $\pm$ 0.006			
		5	0.50	1.000 $\pm$ 0.001	0.998 $\pm$ 0.001	0.985 $\pm$ 0.018	0.992 $\pm$ 0.005	0.890 $\pm$ 0.080	0.971 $\pm$ 0.029	0.994 $\pm$ 0.002			
			0.25	1.000 $\pm$ 0.000	0.999 $\pm$ 0.001	0.991 $\pm$ 0.007	0.994 $\pm$ 0.007	0.959 $\pm$ 0.029	0.969 $\pm$ 0.025	0.997 $\pm$ 0.002			
		16	2	0.50	0.997 $\pm$ 0.003	0.990 $\pm$ 0.003	0.951 $\pm$ 0.011	0.959 $\pm$ 0.023	0.869 $\pm$ 0.082	0.963 $\pm$ 0.019	0.973 $\pm$ 0.003		
			0.25	0.996 $\pm$ 0.001	0.990 $\pm$ 0.003	0.956 $\pm$ 0.016	0.968 $\pm$ 0.019	0.883 $\pm$ 0.115	0.959 $\pm$ 0.017	0.980 $\pm$ 0.007			
		32	5	0.50	1.000 $\pm$ 0.000	0.998 $\pm$ 0.001	0.982 $\pm$ 0.003	0.983 $\pm$ 0.013	0.916 $\pm$ 0.064	0.977 $\pm$ 0.013	0.990 $\pm$ 0.003		
			0.25	1.000 $\pm$ 0.000	0.999 $\pm$ 0.000	0.993 $\pm$ 0.004	0.992 $\pm$ 0.007	0.935 $\pm$ 0.085	0.982 $\pm$ 0.013	0.996 $\pm$ 0.003			
		64	2	0.50	0.996 $\pm$ 0.004	0.991 $\pm$ 0.004	0.938 $\pm$ 0.028	0.968 $\pm$ 0.020	0.840 $\pm$ 0.039	0.940 $\pm$ 0.037	0.967 $\pm$ 0.002		
			0.25	0.997 $\pm$ 0.001	0.994 $\pm$ 0.003	0.961 $\pm$ 0.011	0.982 $\pm$ 0.010	0.896 $\pm$ 0.035	0.936 $\pm$ 0.019	0.982 $\pm$ 0.004			
		128	5	0.50	1.000 $\pm$ 0.000	0.997 $\pm$ 0.001	0.975 $\pm$ 0.013	0.984 $\pm$ 0.010	0.887 $\pm$ 0.030	0.955 $\pm$ 0.030	0.986 $\pm$ 0.004		
			0.25	1.000 $\pm$ 0.000	0.999 $\pm$ 0.000	0.993 $\pm$ 0.003	0.995 $\pm$ 0.003	0.953 $\pm$ 0.024	0.961 $\pm$ 0.015	0.997 $\pm$ 0.003			
		+ CC	64	2	0.50	0.995 $\pm$ 0.003	0.989 $\pm$ 0.003	0.907 $\pm$ 0.015	0.966 $\pm$ 0.010	0.820 $\pm$ 0.051	0.917 $\pm$ 0.023	0.956 $\pm$ 0.003	
			0.25	0.998 $\pm$ 0.000	0.994 $\pm$ 0.002	0.944 $\pm$ 0.015	0.973 $\pm$ 0.015	0.860 $\pm$ 0.048	0.939 $\pm$ 0.017	0.973 $\pm$ 0.005			
		+ CC	64	2	0.50	0.993 $\pm$ 0.003	0.971 $\pm$ 0.008	0.979 $\pm$ 0.006	0.975 $\pm$ 0.007	0.991 $\pm$ 0.004	0.973 $\pm$ 0.011	0.931 $\pm$ 0.008	
			0.25	0.997 $\pm$ 0.001	0.979 $\pm$ 0.008	0.989 $\pm$ 0.003	0.988 $\pm$ 0.003	0.996 $\pm$ 0.001	0.985 $\pm$ 0.004	0.954 $\pm$ 0.009			
GPT-L	No Clustering	-	2	0.50	1.000 $\pm$ 0.000	0.991 $\pm$ 0.001	0.847 $\pm$ 0.009	0.909 $\pm$ 0.003	0.699 $\pm$ 0.006	0.915 $\pm$ 0.014	0.910 $\pm$ 0.003		
			0.25	1.000 $\pm$ 0.000	0.995 $\pm$ 0.001	0.886 $\pm$ 0.006	0.934 $\pm$ 0.006	0.732 $\pm$ 0.011	0.921 $\pm$ 0.015	0.931 $\pm$ 0.004			
		5	0.50	1.000 $\pm$ 0.000	0.998 $\pm$ 0.000	0.885 $\pm$ 0.004	0.933 $\pm$ 0.004	0.726 $\pm$ 0.004	0.924 $\pm$ 0.013	0.927 $\pm$ 0.002			
			0.25	1.000 $\pm$ 0.000	0.995 $\pm$ 0.003	0.999 $\pm$ 0.001	0.998 $\pm$ 0.001	1.000 $\pm$ 0.000	0.993 $\pm$ 0.003	0.986 $\pm$ 0.006			
	+ Clustering	8	2	0.50	0.995 $\pm$ 0.007	0.992 $\pm$ 0.006	0.966 $\pm$ 0.024	0.970 $\pm$ 0.016	0.788 $\pm$ 0.150	0.956 $\pm$ 0.041	0.983 $\pm$ 0.008		
			0.25	0.995 $\pm$ 0.002	0.990 $\pm$ 0.004	0.967 $\pm$ 0.011	0.971 $\pm$ 0.017	0.891 $\pm$ 0.049	0.952 $\pm$ 0.023	0.984 $\pm$ 0.004			
		5	0.50	1.000 $\pm$ 0.001	0.999 $\pm$ 0.001	0.991 $\pm$ 0.010	0.990 $\pm$ 0.007	0.849 $\pm$ 0.123	0.971 $\pm$ 0.031	0.996 $\pm$ 0.002			
			0.25	1.000 $\pm$ 0.000	0.999 $\pm$ 0.001	0.993 $\pm$ 0.008	0.992 $\pm$ 0.010	0.947 $\pm$ 0.039	0.967 $\pm$ 0.032	0.998 $\pm$ 0.001			
		16	2	0.50	0.997 $\pm$ 0.003	0.992 $\pm$ 0.003	0.965 $\pm$ 0.010	0.952 $\pm$ 0.033	0.857 $\pm$ 0.095	0.965 $\pm$ 0.021	0.982 $\pm$ 0.002		
			0.25	0.997 $\pm$ 0.001	0.991 $\pm$ 0.004	0.967 $\pm$ 0.010	0.964 $\pm$ 0.023	0.865 $\pm$ 0.148	0.960 $\pm$ 0.018	0.985 $\pm$ 0.005			
		32	5	0.50	1.000 $\pm$ 0.000	0.999 $\pm$ 0.000	0.988 $\pm$ 0.002	0.978 $\pm$ 0.017	0.903 $\pm$ 0.073	0.978 $\pm$ 0.015	0.993 $\pm$ 0.002		
			0.25	1.000 $\pm$ 0.000	1.000 $\pm$ 0.000	0.994 $\pm$ 0.004	0.991 $\pm$ 0.009	0.920 $\pm$ 0.114	0.980 $\pm$ 0.018	0.997 $\pm$ 0.003			
		128	2	0.50	0.995 $\pm$ 0.005	0.993 $\pm$ 0.004	0.960 $\pm$ 0.019	0.964 $\pm$ 0.026	0.820 $\pm$ 0.048	0.941 $\pm$ 0.042	0.981 $\pm$ 0.004		
			0.25	0.998 $\pm$ 0.001	0.993 $\pm$ 0.002	0.974 $\pm$ 0.006	0.980 $\pm$ 0.013	0.887 $\pm$ 0.046	0.934 $\pm$ 0.022	0.990 $\pm$ 0.004			
		64	5	0.50	1.000 $\pm$ 0.000	0.999 $\pm$ 0.001	0.988 $\pm$ 0.007	0.981 $\pm$ 0.015	0.867 $\pm$ 0.039	0.956 $\pm$ 0.034	0.994 $\pm$ 0.004		
			0.25	1.000 $\pm$ 0.000	0.999 $\pm$ 0.000	0.996 $\pm$ 0.002	0.995 $\pm$ 0.005	0.948 $\pm$ 0.031	0.956 $\pm$ 0.020	0.998 $\pm$ 0.003			
		+ CC	64	2	0.50	0.993 $\pm$ 0.004	0.977 $\pm$ 0.008	0.980 $\pm$ 0.007	0.973 $\pm$ 0.008	0.991 $\pm$ 0.005	0.970 $\pm$ 0.013	0.957 $\pm$ 0.008	
			0.25	0.997 $\pm$ 0.001	0.982 $\pm$ 0.011	0.988 $\pm$ 0.004	0.985 $\pm$ 0.004	0.996 $\pm$ 0.001	0.982 $\pm$ 0.005	0.973 $\pm$ 0.010			
		+ CC	64	2	0.50	0.993 $\pm$ 0.004	0.972 $\pm$ 0.004	0.970 $\pm$ 0.010	0.816 $\pm$ 0.028	0.954 $\pm$ 0.027	0.986 $\pm$ 0.006		
			0.25	0.999 $\pm$ 0.001	0.995 $\pm$ 0.003	0.959 $\pm$ 0.008	0.968 $\pm$ 0.008	0.902 $\pm$ 0.030	0.958 $\pm$ 0.021	0.995 $\pm$ 0.005			
		+ CC	64	2	0.50	0.993 $\pm$ 0.004	0.977 $\pm$ 0.008	0.980 $\pm$ 0.007	0.973 $\pm$ 0.008	0.991 $\pm$ 0.005	0.970 $\pm$ 0.013	0.957 $\pm$ 0.008	
			0.25	0.997 $\pm$ 0.001	0.982 $\pm$ 0.011	0.988 $\pm$ 0.004	0.985 $\pm$ 0.004	0.996 $\pm$ 0.001	0.982 $\pm$ 0.005	0.973 $\pm$ 0.010			
RAR-XL	No Clustering	-	2	0.50	0.996 $\pm$ 0.001	0.961 $\pm$ 0.003	0.744 $\pm$ 0.014	0.875 $\pm$ 0.009	0.679 $\pm$ 0.012	0.890 $\pm$ 0.005	0.885 $\pm$ 0.002		
			0.25	0.998 $\pm$ 0.001	0.977 $\pm$ 0.002	0.788 $\pm$ 0.006	0.904 $\pm$ 0.009	0.709 $\pm$ 0.009	0.908 $\pm$ 0.004	0.904 $\pm$ 0.002			
		5	0.50	0.999 $\pm$ 0.000	0.985 $\pm$ 0.002	0.807 $\pm$ 0.009	0.923 $\pm$ 0.006	0.723 $\pm$ 0.012	0.916 $\pm$ 0.006	0.912 $\pm$ 0.003			
			0.25	1.000 $\pm$ 0.000	0.997 $\pm$ 0.001	0.896 $\pm$ 0.004	0.963 $\pm$ 0.005	0.791 $\pm$ 0.010	0.937 $\pm$ 0.003	0.946 $\pm$ 0.002			
	+ Clustering	8	2	0.50	0.994 $\pm$ 0.005	0.985 $\pm$ 0.007	0.933 $\pm$ 0.034	0.946 $\pm$ 0.020	0.878 $\pm$ 0.038	0.947 $\pm$ 0.023	0.961 $\pm$ 0.013		
			0.25	0.993 $\pm$ 0.005	0.988 $\pm$ 0.007	0.960 $\pm$ 0.019	0.954 $\pm$ 0.015	0.887 $\pm$ 0.044	0.950 $\pm$ 0.024	0.971 $\pm$ 0.014			
		5	0.50	1.000 $\pm$ 0.000	0.999 $\pm$ 0.001	0.985 $\pm$ 0.012	0.989 $\pm$ 0.007	0.955 $\pm$ 0.020	0.975 $\pm$ 0.013	0.990 $\pm$ 0.006			
			0.25	1.000 $\pm$ 0.000	1.000 $\pm$ 0.000	0.998 $\pm$ 0.002	0.997 $\pm$ 0.003	0.980 $\pm$ 0.019	0.986 $\pm$ 0.007	0.997 $\pm$ 0.003			
		16	2	0.50	0.997 $\pm$ 0.001	0.987 $\pm$ 0.004	0.919 $\pm$ 0.045	0.951 $\pm$ 0.021	0.838 $\pm$ 0.056	0.941 $\pm$ 0.018	0.953 $\pm$ 0.010		
			0.25	0.998 $\pm$ 0.001	0.992 $\pm$ 0.002	0.922 $\pm$ 0.038	0.970 $\pm$ 0.012	0.879 $\pm$ 0.041	0.945 $\pm$ 0.009	0.962 $\pm$ 0.013			
		32	5	0.50	1.000 $\pm$ 0.000	0.998 $\pm$ 0.001	0.980 $\pm$ 0.028	0.947 $\pm$ 0.013	0.807 $\pm$ 0.043	0.933 $\pm$ 0.007	0.941 $\pm$ 0.007		
			0.25	0.999 $\pm$ 0.001	0.991 $\pm$ 0.003	0.916 $\pm$ 0.023	0.958 $\pm$ 0.014	0.841 $\pm$ 0.063	0.942 $\pm</math$				



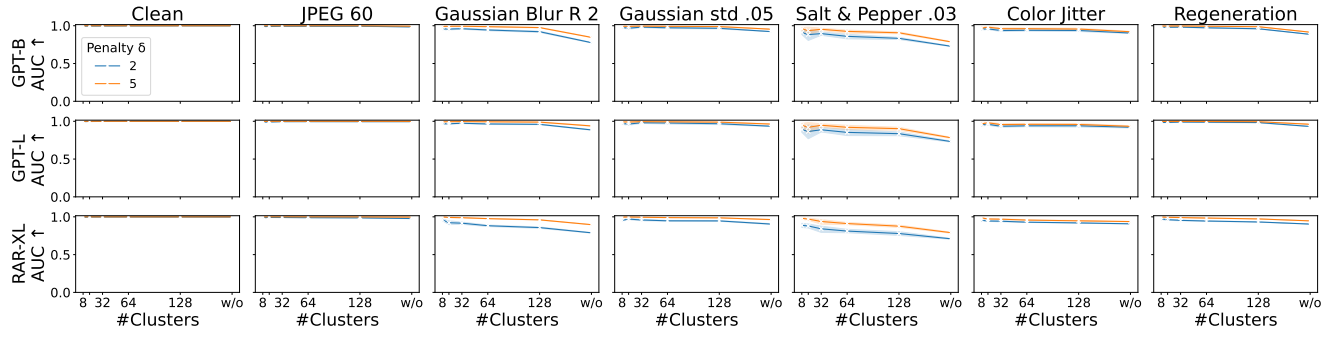
(a) TPR@FPR=1% for green token fraction  $\gamma = 0.5$



(b) TPR@FPR=1% for green token fraction  $\gamma = 0.25$



(c) AUC for green token fraction  $\gamma = 0.5$



(d) AUC for green token fraction  $\gamma = 0.25$

Figure 8. Ablation of detection characteristics across models, perturbations, amount of clusters, penalty  $\delta$ , and green token fraction  $\gamma$  settings. The results are reported over multiple prefixes (8 for RAR-XL as well as LlamaGen GPT-B and GPT-L), where the standard deviation  $\sigma$  is indicated by the colored areas. The lines are averaged over prefixes. Note that the cluster classifier is not used here. The corresponding data with mean and  $\sigma$  can be found in Tables 8 and 9.

### Llamagen B



Figure 9. Visual examples of unwatermarked and watermarked images generated with **LlamaGen (GPT-B)** across different settings.

### Llamagen L

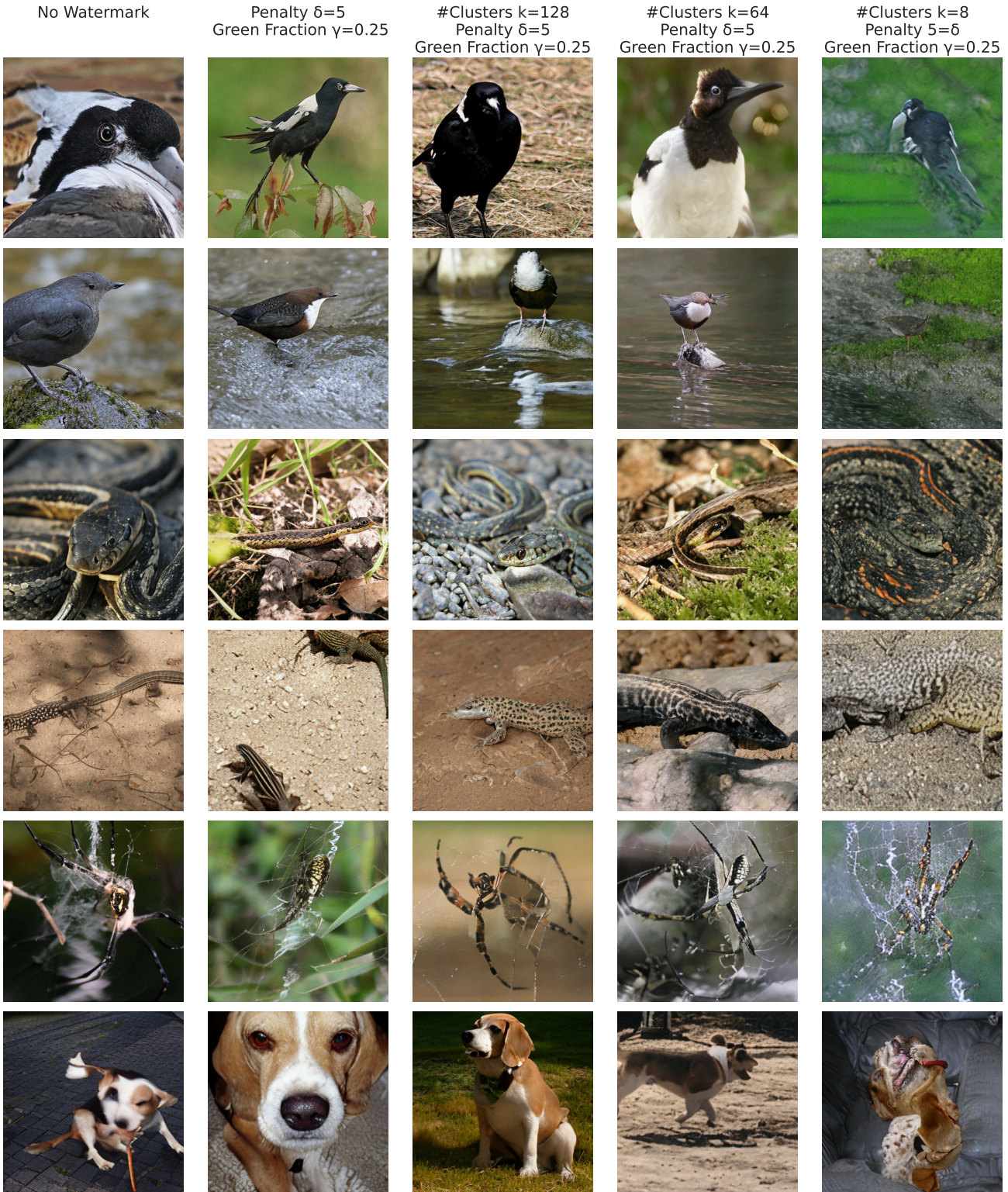


Figure 10. Visual examples of unwatermarked and watermarked images generated with **LlamaGen (GPT-L)** across different settings.

### RAR XL



Figure 11. Visual examples of unwatermarked and watermarked images generated with **RAR-XL** across different settings.